Orthogonally self-sorted hydrogels with pathway-dependent morphology guide bimetallic nanozyme formation

*Debolina Saha, Shreya Sridhar, Ipsita Sahu, and Priyadarshi Chakraborty**

Department of Chemistry
Indian Institute of Technology Hyderabad
Kandi, Sangareddy 502284, Telangana, India
Corresponding author E-mail: priyadarshi@chy.iith.ac.in

Materials

Folic acid (FA), Sodium borohydride, TMB, Silver nitrate, Gold chloride hydrate, Methylene Blue, and Methyl Orange were purchased from SRL. H_2O_2 was purchased from Sigma Aldrich. FmocFF was purchased from BLD Pharma. They were used as received.

Methods

Preparation of FmocFF hydrogel:

FmocFF hydrogel was prepared using the solvent-switch method. Fmoc-FF was first dissolved in DMSO (100 mg/mL) to make the 10% stock solution. The required amount of stock was diluted in equal volume (*v/v*) DMSO-water mixture to induce gelation. The final concentration of FmocFF in the hydrogel (FmocFF-SW) was 0.27% (*w/v*). The gel formation was confirmed by vial inversion.

Preparation of FA hydrogel:

FA hydrogel was prepared by mixing FA stock (0.75% (*w/v*)) in DMSO at 80 °C followed by dilution of water in a DMSO-water volume ratio of 1:1 to induce gelation. The final concentration of FA in the hydrogel (FA-SW) was 0.23% (*w/v*). The gel formation was confirmed by vial inversion.

Preparation of FmocFF/FA multicomponent hydrogels by solvent-switch method (SS-SW):

SS-SW hydrogels were prepared by the solvent-switch method. Stock solutions of FmocFF (10% (*w/v*)) and FA (0.75% (*w/v*)) in DMSO were prepared. An appropriate volume of each stock solution was diluted to obtain the molar ratio of Fmoc-FF and FA 1:1, 1:2, 1:3, 2:1, and 3:1 in DMSO-water mixture to obtain the solvent composition as 1:1, leading to the final hydrogel concentration 0.5% (*w/v*).

Preparation of FmocFF/FA multicomponent hydrogels by heating-cooling method (SS-HC):

SS-HC hydrogels were prepared by heating the gel prepared by aforementioned solvent switch method after overnight incubation. The gels were heated at 70°C to sol-phase ensuring homogeneity and were allowed to cool to room temperature. The final solvent composition and molar ratio of gelators remained same as described previously.

Preparation of SS-SW/Ag hybrid gel:

SS-SW/Ag nano-hybrid gel was prepared by diluting the stock solution of FmocFF (10% (*w/v*)) and FA (0.75% (*w/v*)) to 1:1 mixture of DMSO-water followed by the addition of aqueous Ag^+ solution from 50 mM stock solution to make the final concentration of Ag^+ solution 0.025% (*w/v*). The solution was then vortexed and kept under diffused sunlight until the formation of silver nanoparticles which was confirmed by color change from yellow to orange.

Preparation of SS-SW/Au nano hybrid gel:

SS-SW/Au nano hybrid gel was prepared by mixing FmocFF and FA stock followed by dilution with DMSO-water 1:1 ratio. A calculated volume of an aqueous Au^{3+} solution from 25mM stock solution was added to achieve a final concentration of Au^{3+} solution 0.025% (*w/v*), and the mixture was vortexed thoroughly, allowed to form gel, then kept at 45˚C to promote *in-situ* gold nanoparticles formation. It was confirmed by visible colour change from yellow to dark pink.

Preparation of SS-SW/Au/Ag nano-hybrid gel:

Au/Ag nano-hybrid hydrogel was prepared by adding both the aqueous Ag^+ solution and Au^{3+} solution to the SS-SW gel. For this, during the preparation of SS-SW hydrogel (as mentioned above) both Au^{3+} (0.0125% *w/v*) and Ag^+ (0.0125% *w/v*) aqueous solutions were added to hydrogel formulation in equal amount (both Au^{3+} and Ag^+ solution 0.0125% *w/v*). The solution was then vortexed and kept under diffused sunlight followed by heating at 45˚C. Final concentration of Au^{3+}/Ag^+ solution 0.025% *w/v*. The nanoparticle formation was confirmed by color change from yellow to dark purple.

Catalytic activity of nano-hybrid gels:

Peroxidase activity

The Peroxidase activity was evaluated by using a TMB-H_2O_2 colorimetric assay. A 10 mM stock solution of TMB in DMSO and 0.20 M stock solution of H_2O_2 in water were prepared initially. The reaction mixture was prepared by mixing 10 mM TMB and 0.2 M of H_2O_2 in acetate buffer (pH = 4.5) leading to the final TMB and H_2O_2 concentration of 0.5 mM and 5mM respectively. The reaction mixture was then added on top of the nano-hybrid gels (SS-SW/Ag, SS-SW/Au, SS-SW/Ag/Au) to monitor the oxidation of TMB by detecting the absorption at 654 nm as a function of time up to 60 min. The same study was carried out for

SS-SW system as well as without any gel (control). The catalytic reaction occurred on the gel surface, resulting in the formation of a blue-coloured solution. Kinetic measurements were carried out by monitoring the time-dependent change in absorbance at 654 nm using different concentrations of TMB (0.5, 1, 1.5 and 2 mM) in the reaction mixture. For the peroxidase-like activity, apparent Michaelis-Menten parameters were determined by initial-rate analysis. Time-dependent absorbance data were recorded at different TMB concentrations, and each experiment was performed in triplicate. Initial rates were extracted from the early linear region of the reaction profiles. The initial rates were then plotted against substrate concentration (TMB), including error bars, and fitted to the Michaelis-Menten equation using nonlinear regression (OriginPro 2025 software). Nonlinear fitting was chosen because it provides more accurate and statistically robust estimates of K_m and V_{max} than linearization methods.[1-3]

Dye degradation

For dye degradation experiments, stock solutions (2 mM) of Methylene Blue (MB) and Methyl Orange (MO) were diluted with water to obtain final concentrations of 0.25 mM (MB) and 0.5 mM (MO). A freshly prepared $NaBH_4$ solution (700 µL, 5 mM) was added to 700 µL of the dye solution, and the resulting mixture was carefully placed on top of the hydrogel (1 mL) to initiate catalytic degradation. The degradation was monitored by periodically withdrawing 1 mL of the supernatant for UV-Vis spectroscopic analysis. Absorbance at 664 nm and 464 nm was used to calculate the % degradation for MB and MO, respectively. After measurement, the solution was gently returned to the top of the gel, ensuring minimal disturbance to the gel network. The degradation process was monitored for 30 mins for each dye.

Transmittance Electron Microscopy (TEM):

Hydrogel samples were diluted 20 times and 20 µL was drop cast onto 400-mesh copper grids coated with a carbon-stabilized Formvar film. Grids were air dried and images were acquired using a JEOL JEM-2100FX transmission electron microscope operated at an accelerating voltage of 80 kV. Energy-dispersive X-ray spectroscopy (EDS) and TEM images of nanoparticles were recorded using the same microscope operated at 80 kV.

X-ray Diffraction (XRD):

The hydrogel samples were drop-cast onto clean glass slides and dried at room temperature. X-ray diffraction studies were carried out by using a Bruker D8 Discover diffract meter equipped with a Cu-Kα radiation source (λ = 1.5406 Å), scanning over a 2θ range of 5° to 90°.

Fourier Transform Infrared (FTIR) Spectroscopy:

The infrared spectra of the dried hydrogel samples were recorded using a Bruker Alpha FTIR spectrometer.

Sample name	***Conc. of gelators (% w/v)***	***pH***
FmocFF-SW	0.27	3.8 ± 0.5
FmocFF-HC	0.27	3.16 ± 0.2

Rheology:

The viscoelastic behaviour of hydrogels was assessed using Anton Paar MCR301 fitted with a 20 mm parallel-plate geometry and a fixed gap of 0.5 mm.

UV−Vis Absorbance:

UV−Vis absorbance spectra were measured by using a JASCO V-730 spectrophotometer under ambient condition.

Fluorescence Spectroscopy:

Fluorescence measurements of the hydrogel at different concentrations were performed using a Horiba Jobin Yvon spectrofluorometer. Samples were loaded into screw-capped quartz cuvettes with a 1 cm optical path length. The excitation wavelength was set to 269 nm, and emission spectra were collected and the instrument settings included a slit width of 10 nm.

FA-SW	0.23	4.13 ± 0.4
FA-HC	0.23	3.77 ± 0.7
SS-SW (1:1)	0.5	3.96 ± 0.4
SS-HC (1:1)	0.5	3.71 ± 0.1

Table S1. Average pH values of pristine and self-sorted hydrogels prepared by solvent-switch and heating-cooling methods.

Supporting Note 1: The pH values of the pristine FmocFF-SW and FA-SW were measured to be 3.8 and 4.13, respectively. The self-sorted gels exhibited pH values of 3.96 and 3.71 for the SS-SW and SS-HC gels, respectively, reflecting that the pH of the multicomponent system remains within a narrow range relative to the individual gels. This minor variation is unlikely to cause large differences in the protonation state of gelators. The consistent spectroscopic signatures and independent thermal transitions confirm that the observed differences originate from self-sorted assembly rather than pH effects alone.

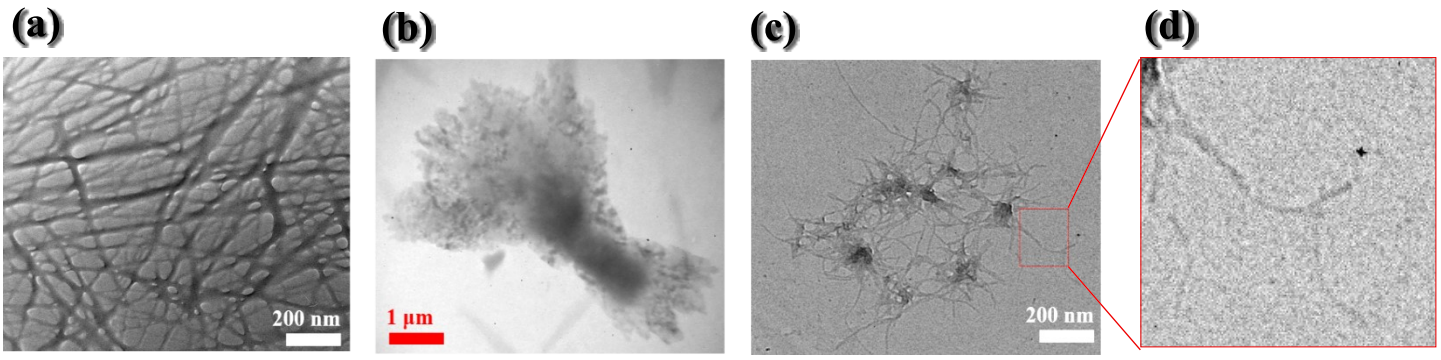

Fig. S1. TEM images showing the nanostructures of (a) FmocFF-SW at 0.27% *w/v* obtained after a heating-cooling cycle (b) and FA-SW hydrogel at 0.23% *w/v* (c) FA-SW hydrogel at 0.23% *w/v* after heating-cooling cycle, and (d) Magnified view of a single fiber of FA highlighted in the TEM image in panel c showing an apparent helical pattern.

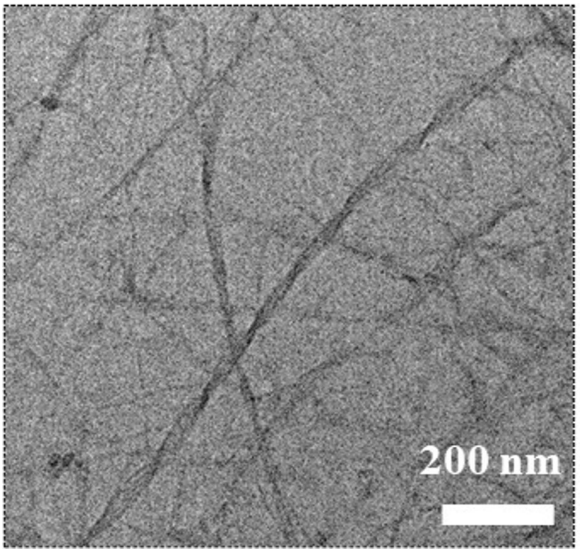

Fig. S2. TEM image showing the nanostructures of SS-HC hydrogel at 0.5% *w/v* showing helical like organization.

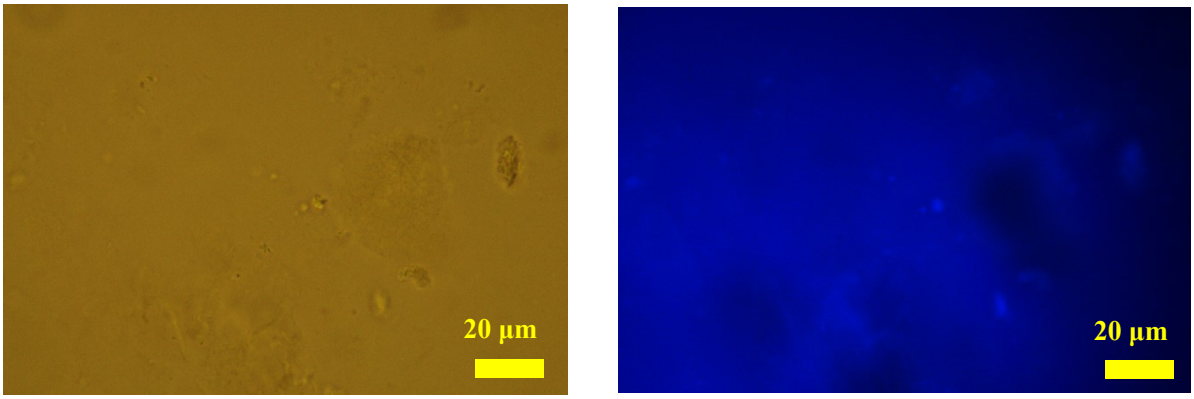

Fig. S3. Bright-field and fluorescence microscopy images of the FmocFF-SW self-assembly (0.27% *w/v*; diluted 20 times).

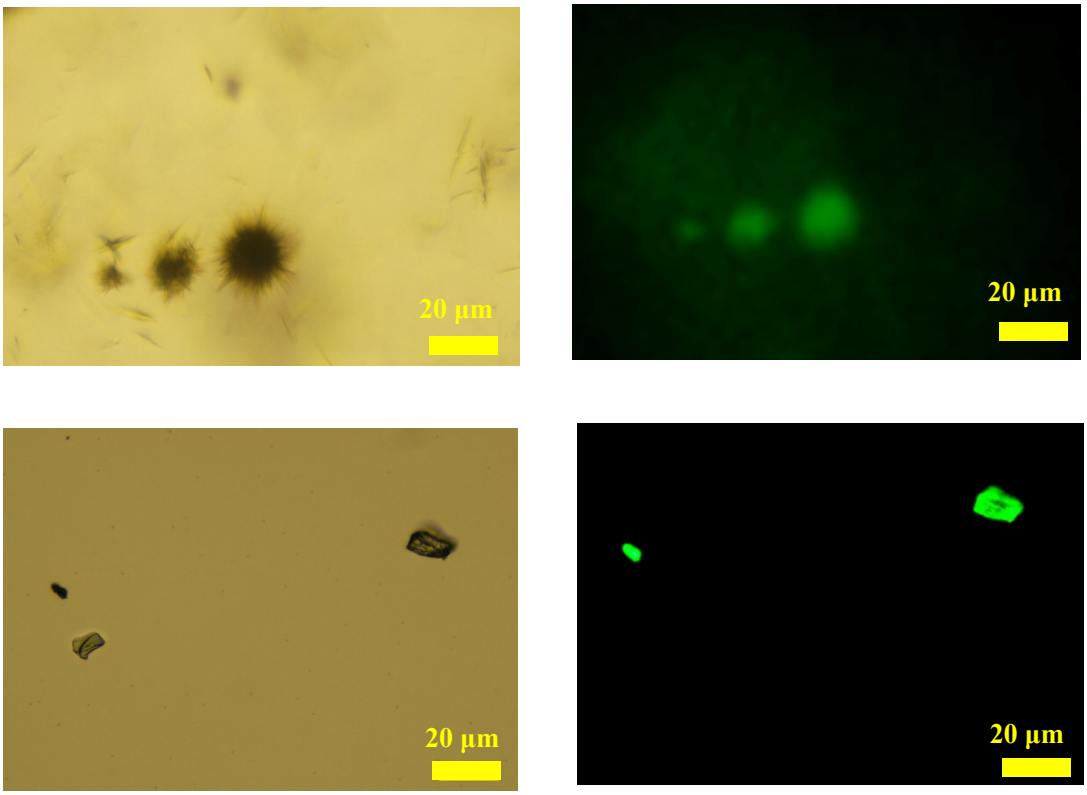

Fig. S4. Bright-field and fluorescence microscopy images of the FA-SW self-assembly (0.23% *w/v*; diluted 20 times).

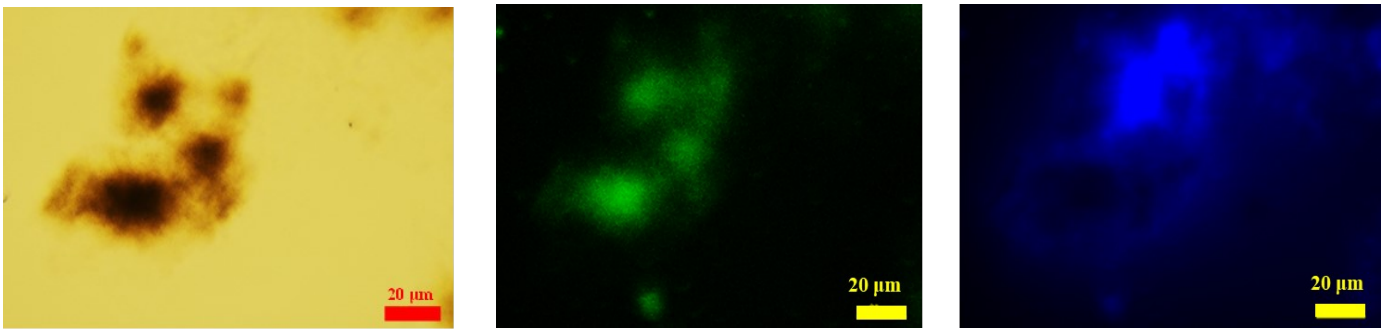

Fig. S5. Bright-field microscopy image and fluorescence microscopy images of the SS-SW hydrogel (1:1 molar ratio at 0.5% *w/v*; diluted 20 times in Milli-Q water) prepared by solvent-switch method [FmocFF exhibited blue fluorescence while FA exhibited green fluorescence].

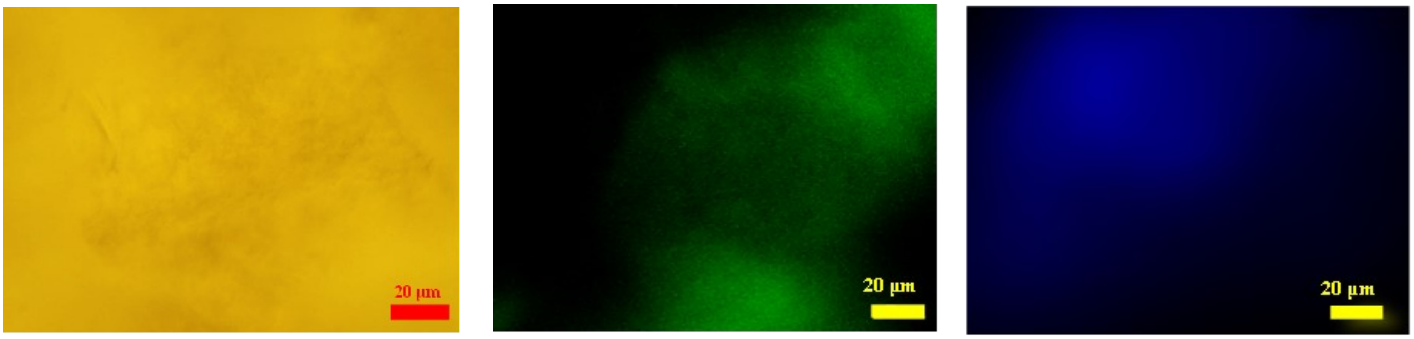

Fig. S6. Bright-field microscopy image and fluorescence microscopy images of the SS-HC hydrogel (1:1 molar ratio at 0.5% *w/v*; diluted 20 times in Milli-Q water) prepared by heating-cooling method [FmocFF exhibited blue fluorescence while FA exhibited green fluorescence].

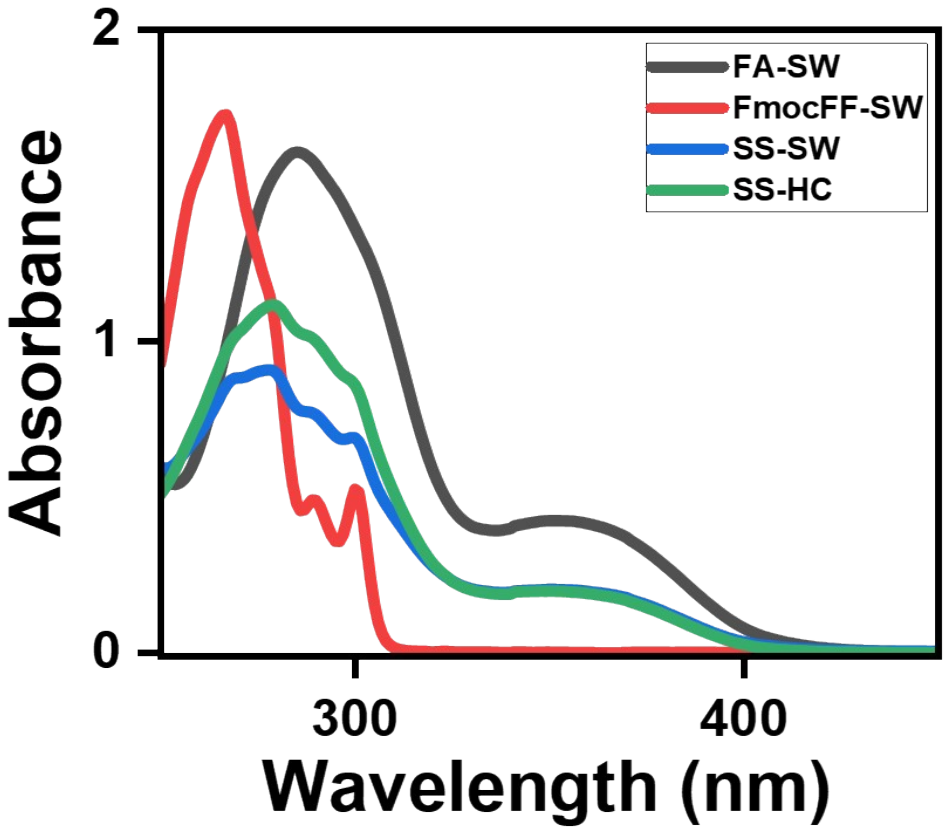

Fig. S7. UV-vis absorbance spectra measured for FmocFF-SW hydrogel (0.27% *w/v* (red)), FA-SW hydrogel (0.23% *w/v* (black)), multicomponent gel prepared by solvent-switch method (0.5% *w/v* (blue)) and heating-cooling at 70°C (0.5% *w/v* (green)) (all hydrogel samples were diluted 20 times in Milli-Q water).

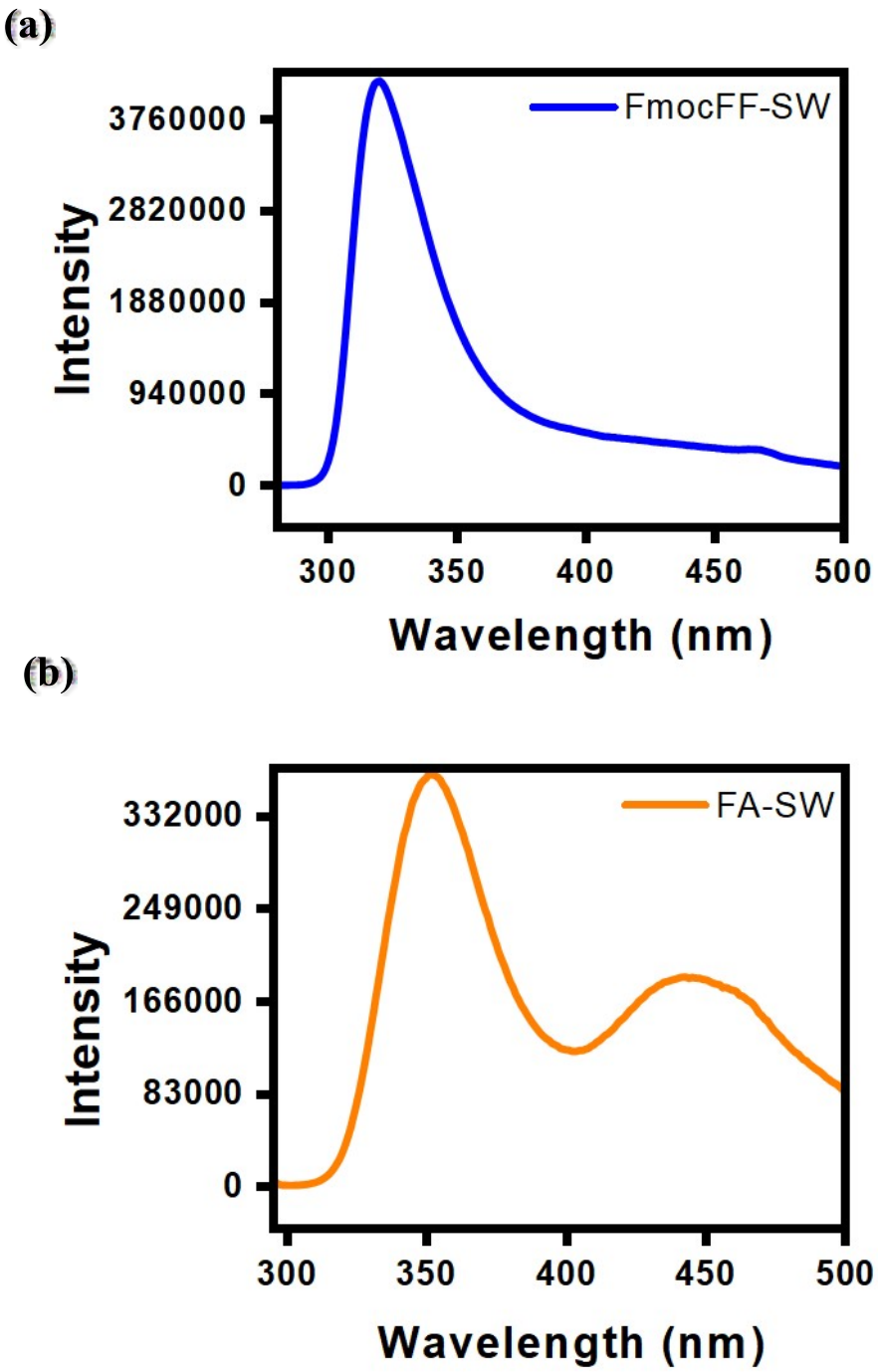

Fig. S8. Fluorescence spectra of pristine (a) FmocFF-SW hydrogel (0.27% w/v; λ_{ex} = 267nm) and (b) FA-SW hydrogel (0.23% w/v; λ_{ex} = 285 nm) prepared by the solvent-switch method.

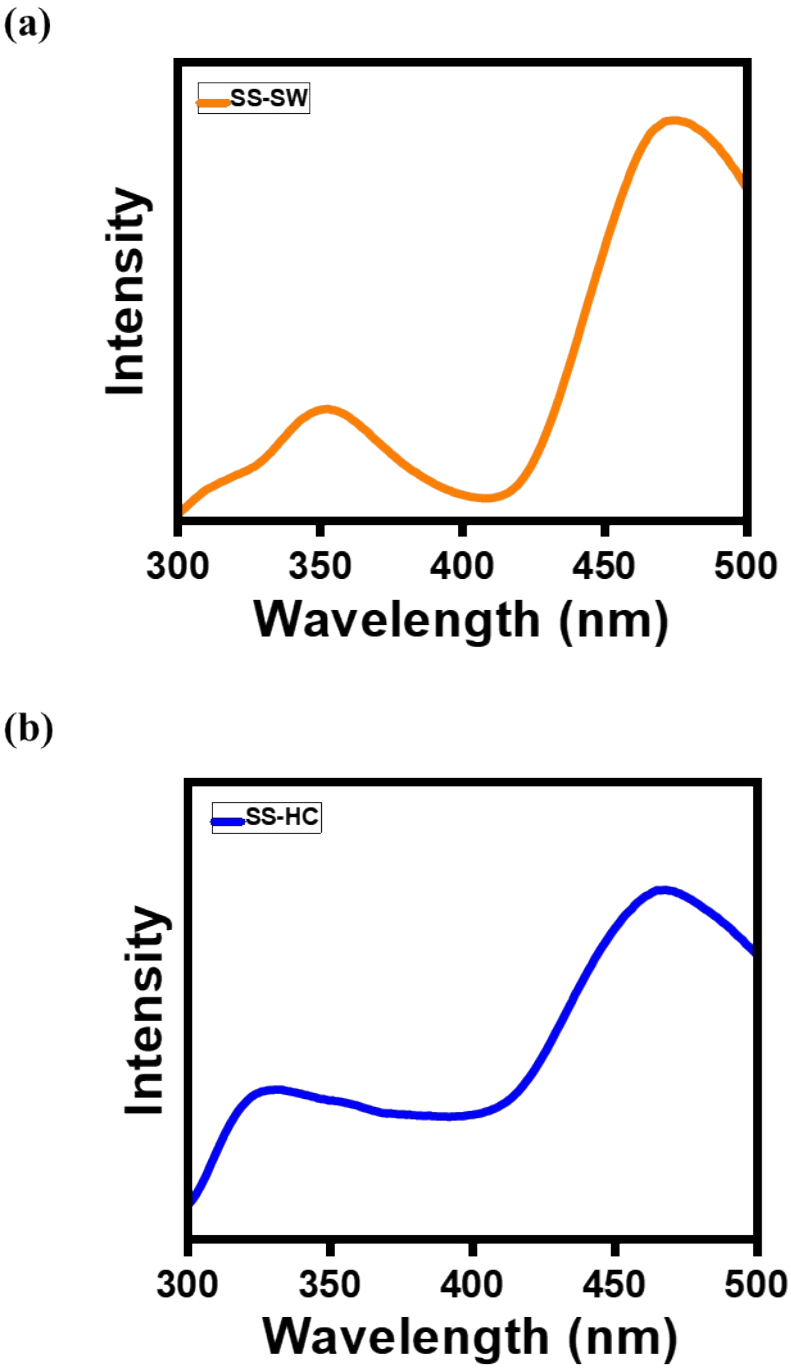

Fig. S9. Fluorescence spectra of (a) SS-SW hydrogel (0.5% w/v) and (b) SS-HC hydrogel (0.5% w/v); both λ_{ex} = 269 nm.

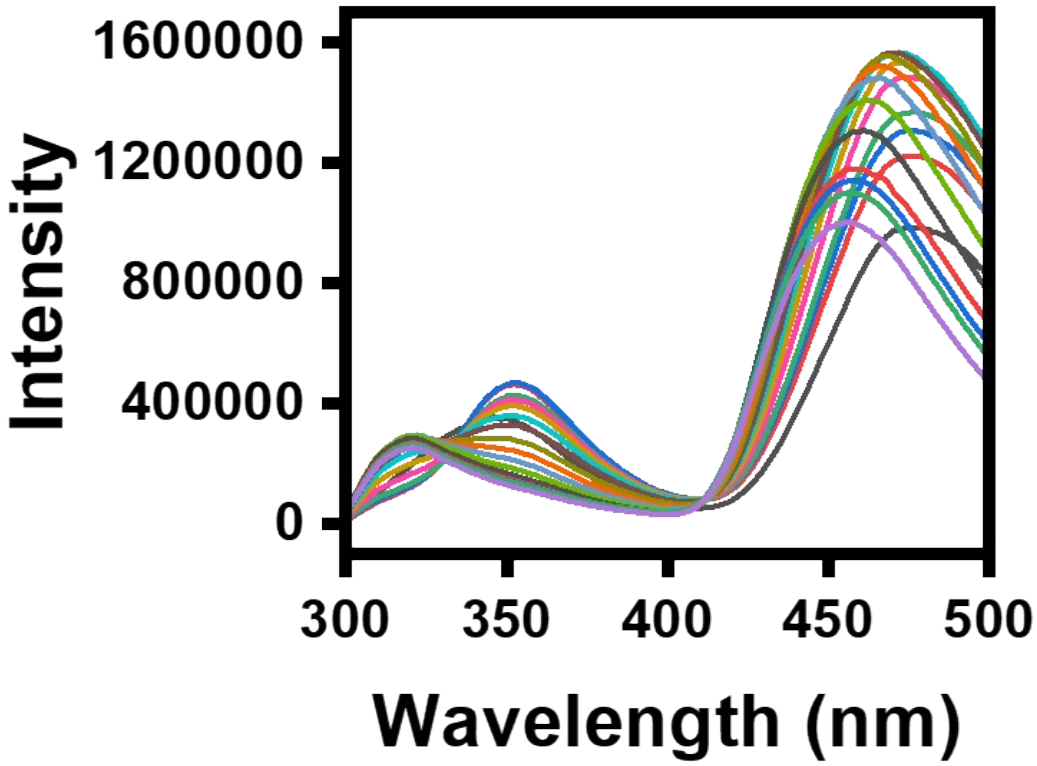

Fig. S10. Temperature-dependent fluorescence spectra of SS-SW hydrogel (0.5% w/v; λ_{ex} = 269 nm) recorded over the range 10 ˚C to 90 ˚C at 5 ˚C intervals.

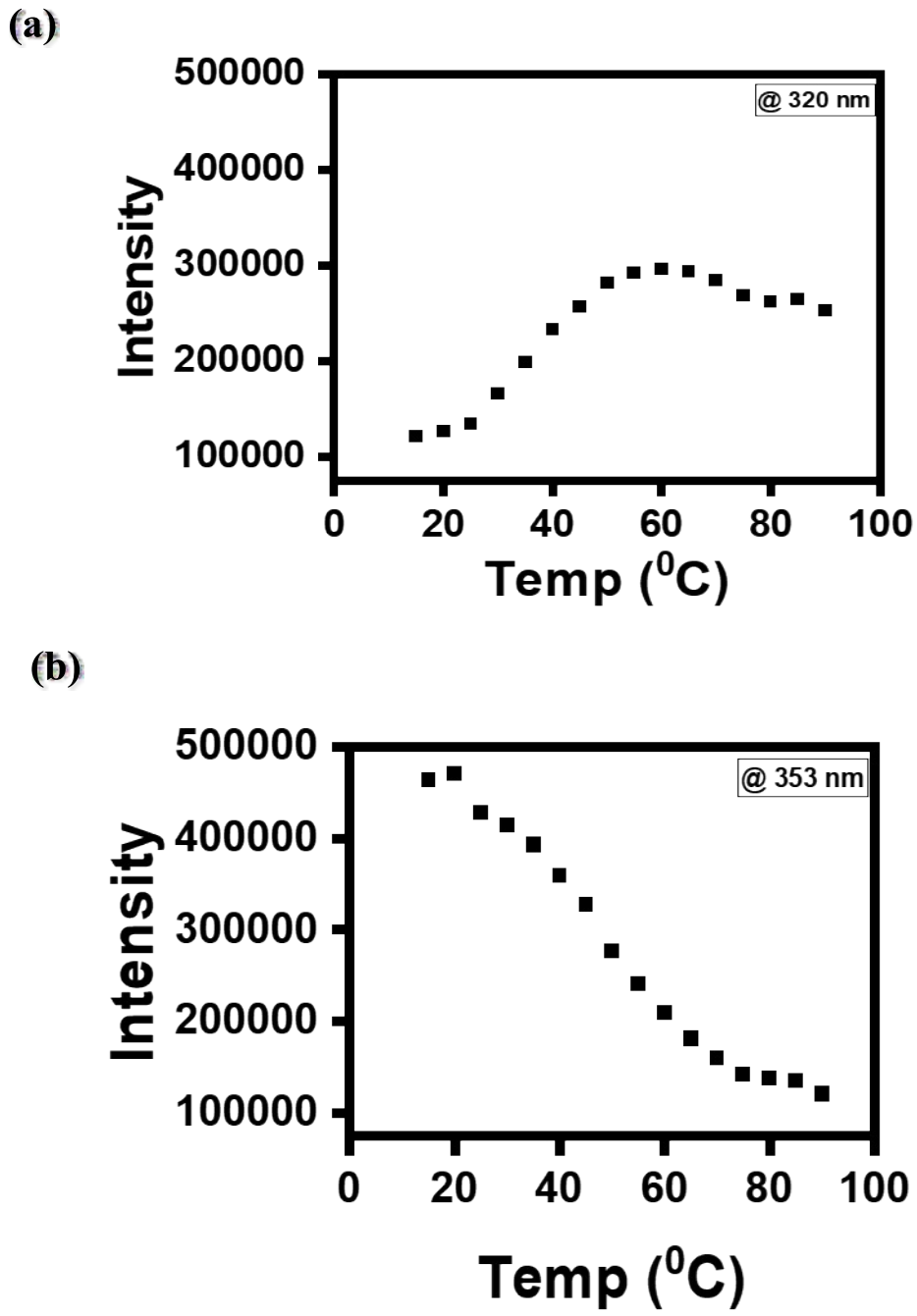

Fig. S11. Plots of fluorescence intensity versus temperature for the SS-SW (0.5% w/v; λ_{ex} = 269 nm) hydrogel at (a) 320 nm and (b) 353 nm.

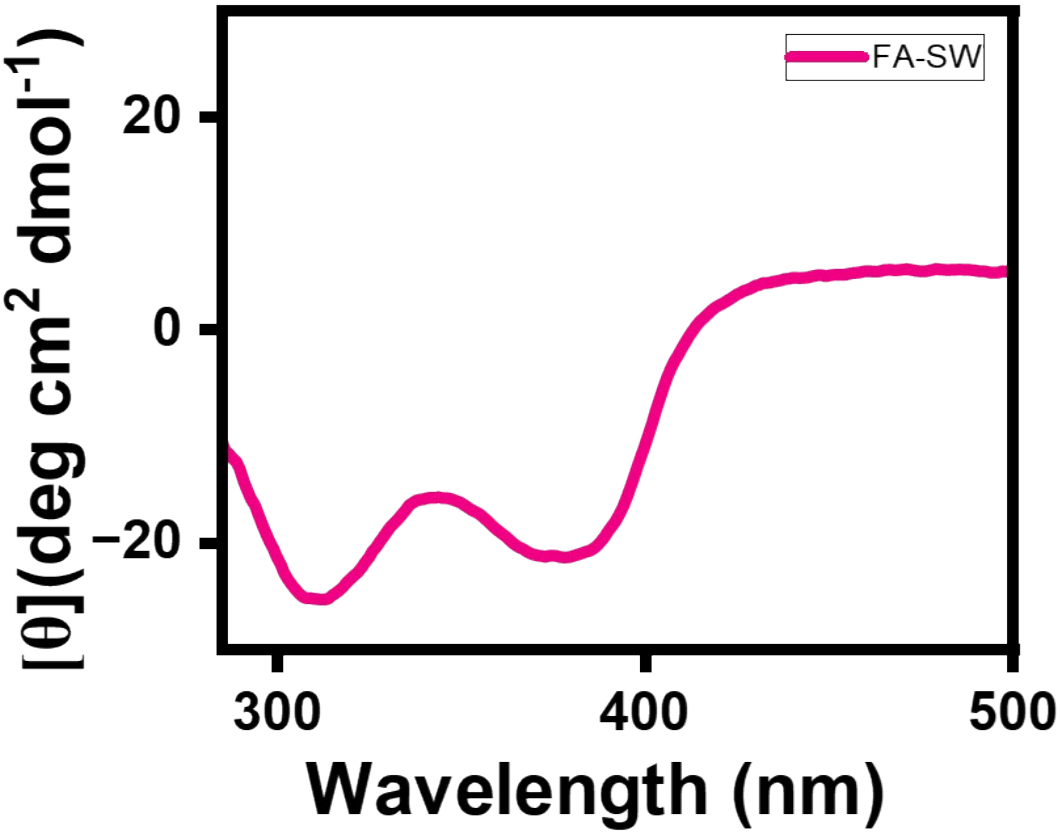

Fig. S12. CD spectra of FA-SW hydrogel (0.23% *w/v*) (hydrogel sample was diluted 20 times in Milli-Q water).

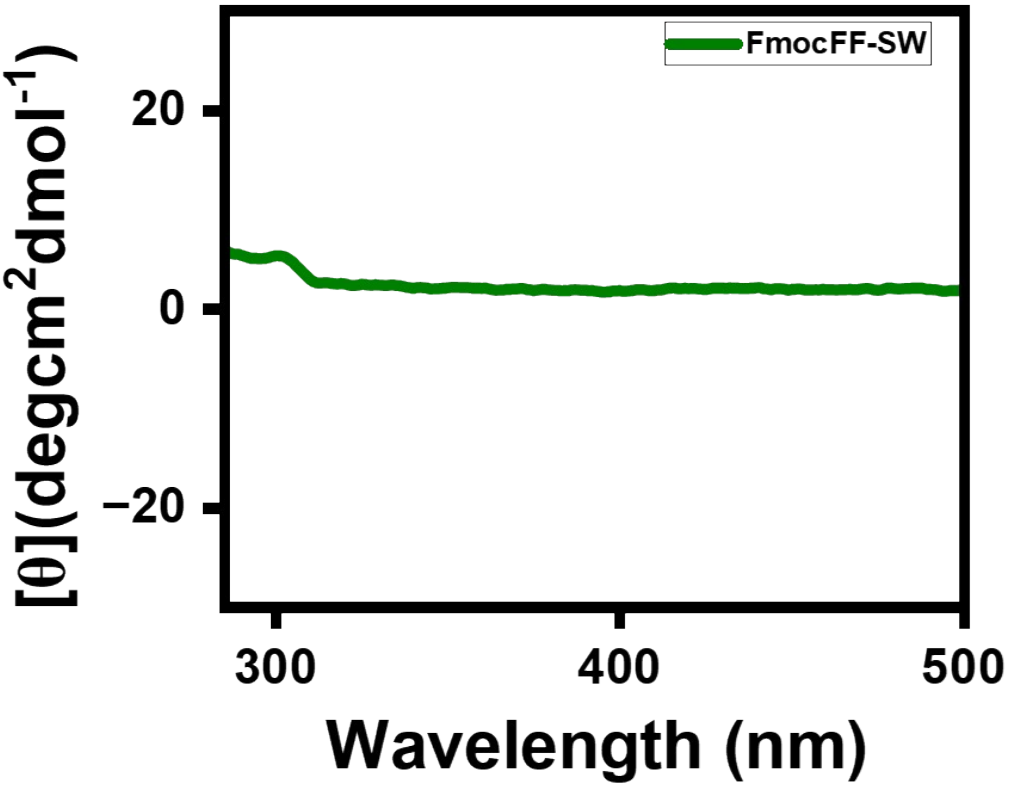

Fig. S13. CD spectra of FmocFF-SW hydrogel (0.27% *w/v*) (hydrogel sample was diluted 20 times in Milli-Q water).

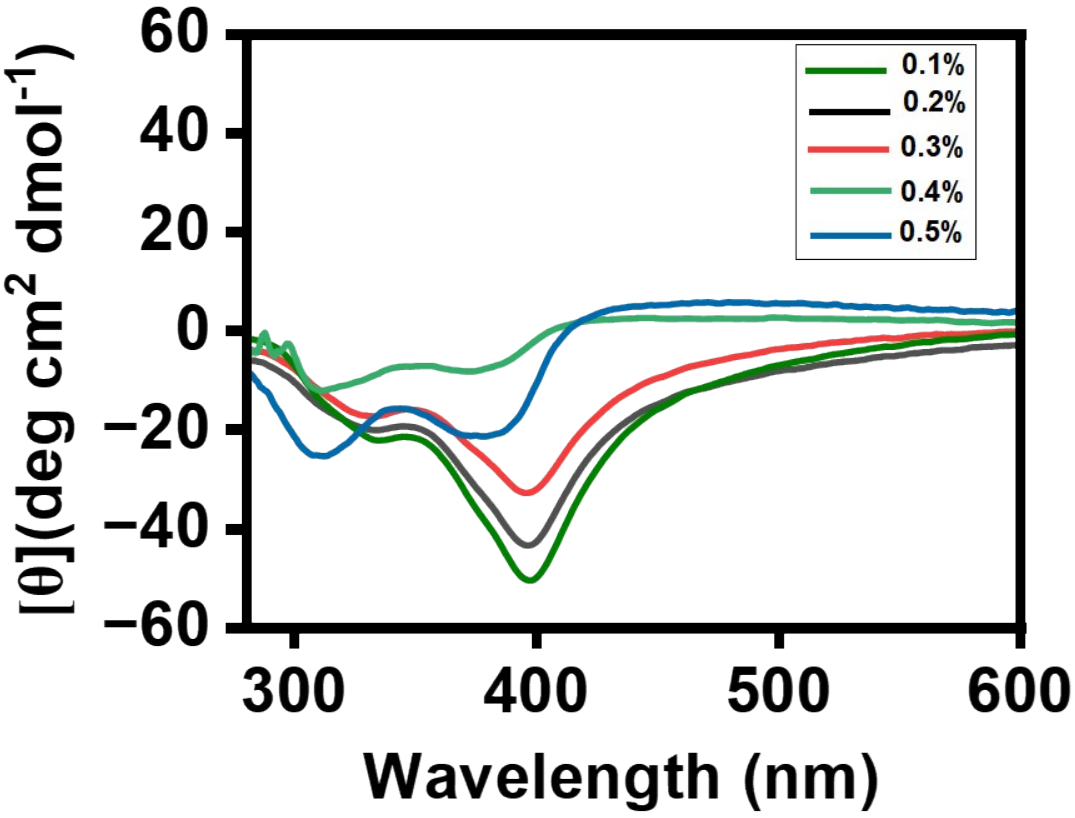

Fig. S14. CD spectra of FA-SW hydrogel at varying concentrations (0.1% to 0.5% *w/v*) (hydrogels were first prepared and diluted 20 times in Milli-Q water).

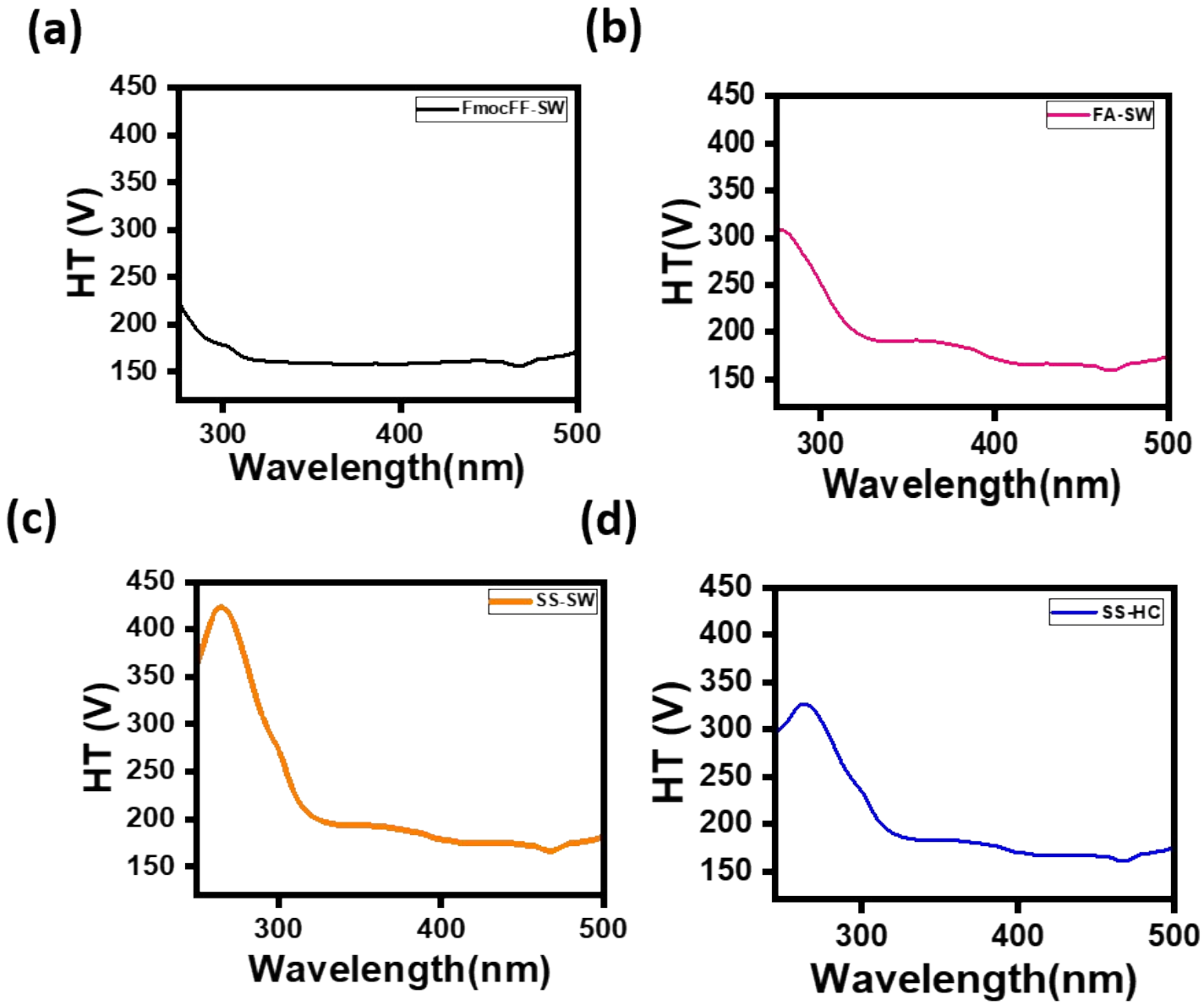

Fig. S15. HT voltage vs. wavelength graphs for (a) FmocFF-SW (0.27% *w/v*) (b) FA-SW (0.23% *w/v*), (c) SS-SW (0.5% *w/v*), and (d) SS-HC (0.5% *w/v*) hydrogels.

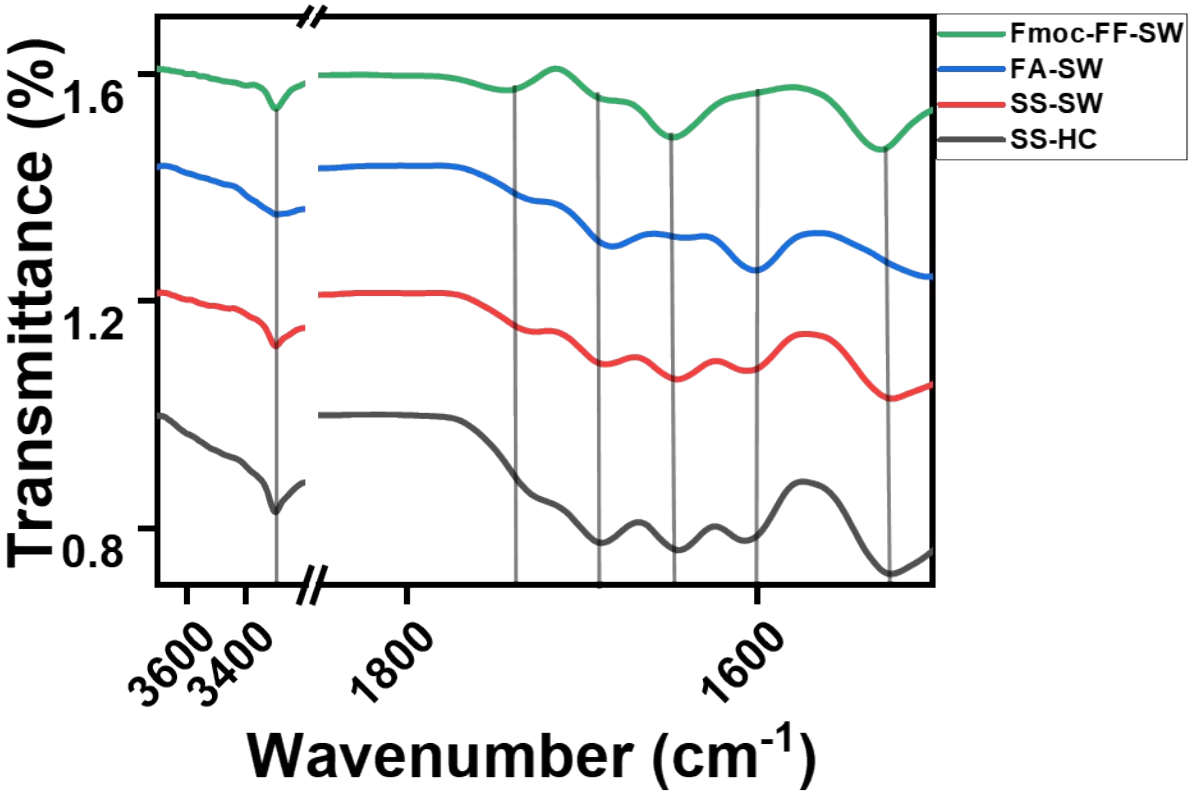

Fig. S16. FTIR spectra of dried FmocFF-SW (0.27% *w/v*; green) (b) FA-SW (0.23% *w/v*; blue), (c) SS-SW (0.5% *w/v*; red), and (d) SS-HC (0.5% *w/v*; black) hydrogels.

Supporting Note 2. In pristine FA-SW gel, distinct peaks are observed at ~1731, 1682-1690, and ~1599 cm^{-1}. Pristine FmocFF-SW shows characteristic bands at ~3301, 1746, 1686, 1648, and 1526 cm^{-1}. In the multicomponent SS-SW and SS-HC gels, peaks from both FA-SW and FmocFF-SW are retained. The multicomponent gels display combined bands at 3300-3305, 1725-1727, 1686-1690, 1642-1644, 1605-1607, and ~1526 cm^{-1}, indicating the presence of features from both components within the assembled networks.

Table S2. Study of frequency-dependent oscillatory rheology of 0.5% *w/v* hydrogels at different concentrations prepared by both solvent-switch (SS-SW) and heating-cooling (SS-HC) methods.

Ratio	Method	G' (Pa)	G" (Pa)
FmocFF+FA (1:1)	Solvent Switch	1028 ± 28	294 ± 7
FmocFF+FA (1:1)	Heating-cooling	2464 ± 40	469 ± 17
FmocFF+FA (1:2)	Solvent Switch	210 ± 17	469 ± 8
FmocFF+FA (1:2)	Heating-cooling	1532 ± 97	400 ± 17
FmocFF+FA (1:3)	Solvent Switch	55 ± 1	15
FmocFF+FA (1:3)	Heating-cooling	549 ± 4	113 ± 0.5
FmocFF+FA (2:1)	Solvent Switch	9541 ± 929	1505 ± 41
FmocFF+FA (2:1)	Heating-cooling	13009 ± 577	2240 ± 216
FmocFF+FA (3:1)	Solvent Switch	17659 ± 1026	3243 ± 217
FmocFF+FA (3:1)	Heating-cooling	22615 ± 822	4088 ± 116

Supporting Note 3. Rheological characterization was also performed on samples with compositions deviating from the equimolar (1:1) ratio. The measured storage modulus (G′) and loss modulus (G″) values are mentioned in the table here. A systematic increase in the fraction of FmocFF leads to a corresponding enhancement in mechanical strength, whereas increasing the proportion of FA results in a progressive reduction in these properties, establishing the role of each component in governing network integrity. Following thermal treatment of all systems, as described in the main text, a consistent increase in G’ was observed across all compositions, indicating thermally induced structural reinforcement.

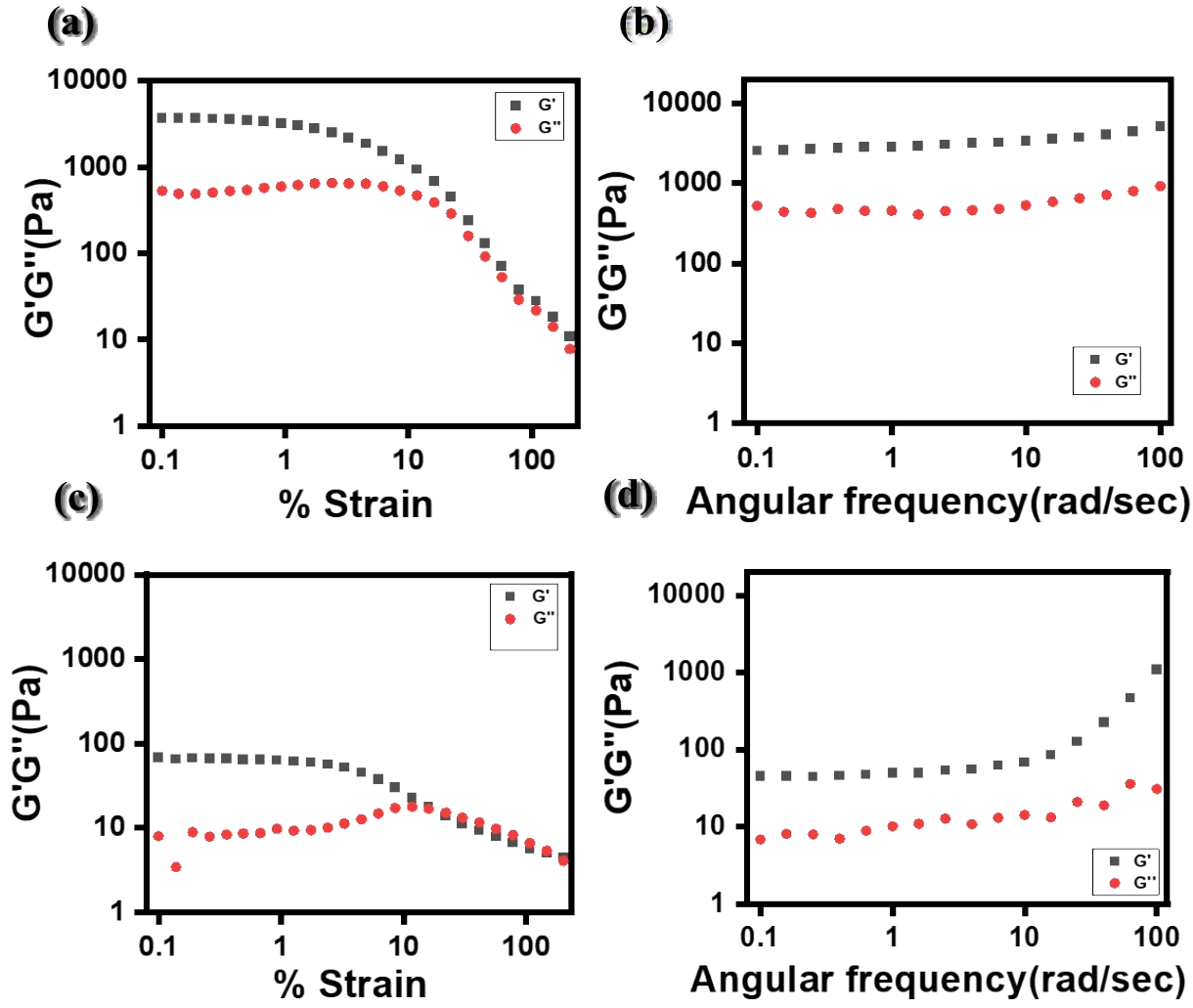

Fig. S17. (a, c) Amplitude sweep experiment was carried out on the FmocFF-SW (0.27% *w/v*) and FA-SW (0.23% *w/v*) hydrogel at 1 Hz frequency. Frequency-sweep measurement was conducted for the (b) FmocFF-SW (0.27% *w/v*) and (d) FA-SW (0.23% *w/v*) hydrogel at 0.1% strain.

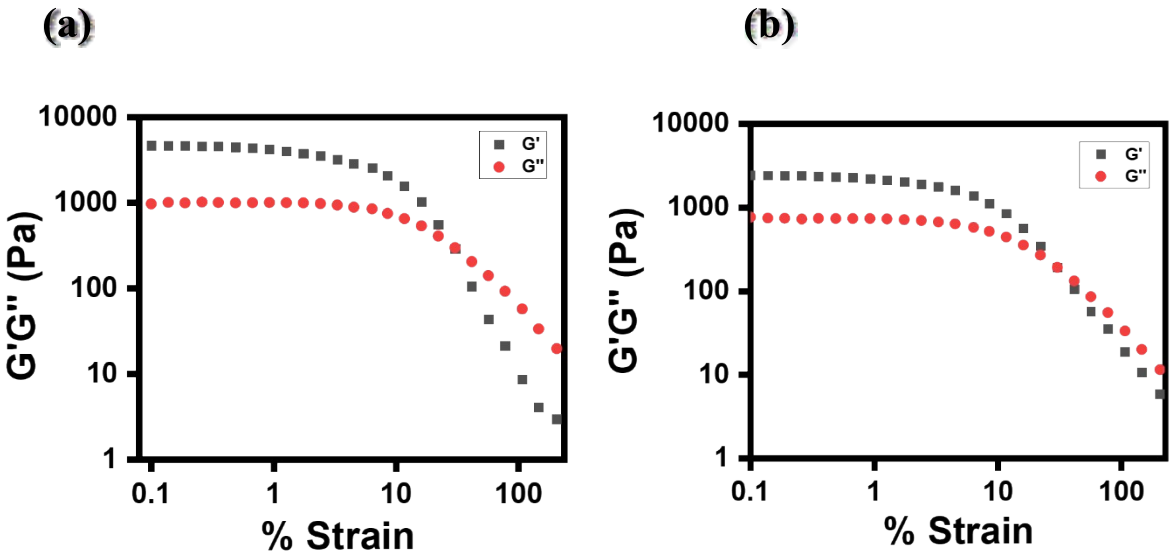

Fig. S18. Strain sweep experiment was carried out on the (a) SS-SW hydrogel (0.5% *w/v*) (b) SS-HC hydrogel (0.5% *w/v*) at 1 Hz frequency.

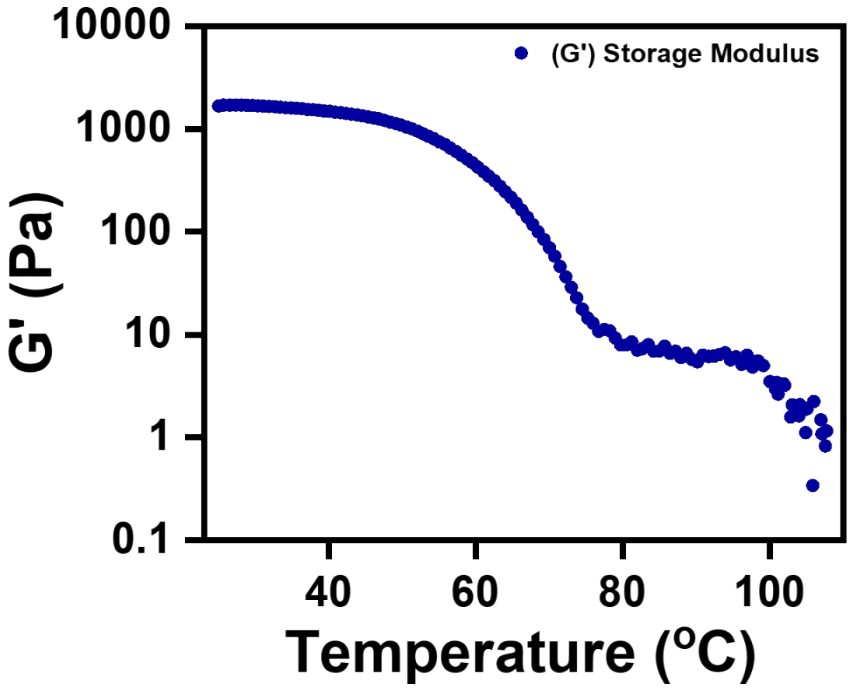

Fig. S19. Temperature Sweep experiment of SS-SW hydrogel from 30°C to 120°C with a ramp of 1°C/min.

Supporting Note 4: Temperature-sweep rheological measurements of the self-sorted hydrogels (Figure S19) showed a two-stage decrease in mechanical strength, with transitions at ~75 °C and ~90 °C. These two transitions are consistent with the differential thermal stability of the individual networks. The first decrease (~75 °C) is attributed to disruption of the FA-SW network, which exhibits comparatively lower mechanical strength, while the second transition (~90 °C) corresponds to the breakdown of the more robust FmocFF-SW network.

This interpretation is supported by DSC analysis, which features two distinct endothermic peaks at ~70 °C and ~91 °C, corresponding to FA-SW and FmocFF-SW, respectively. The close agreement between rheological and calorimetric data supports the presence of two independently assembled networks within the gel.

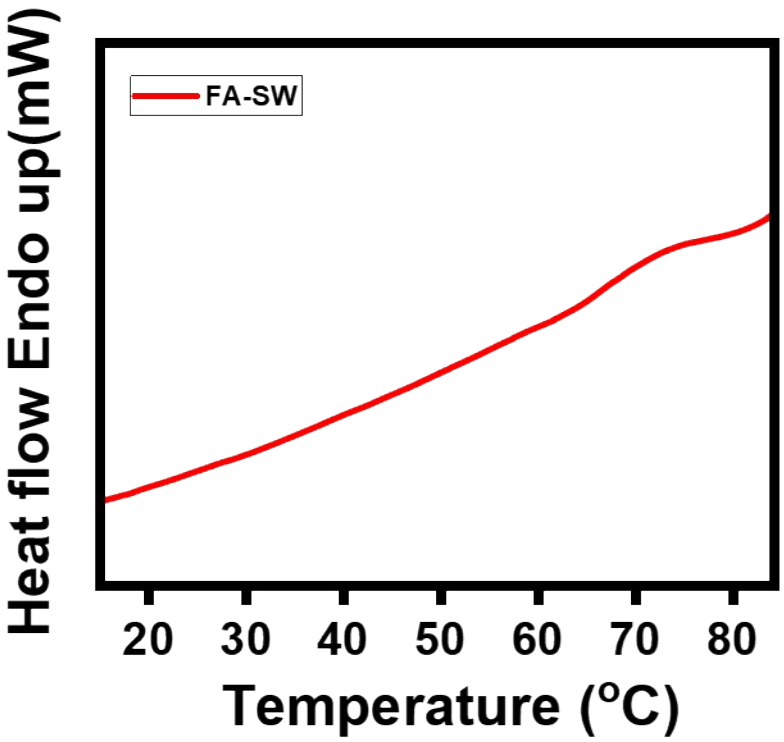

Fig. S20. Differential Scanning Calorimetry curve for FA-SW hydrogel at 0.23% *w/v*.

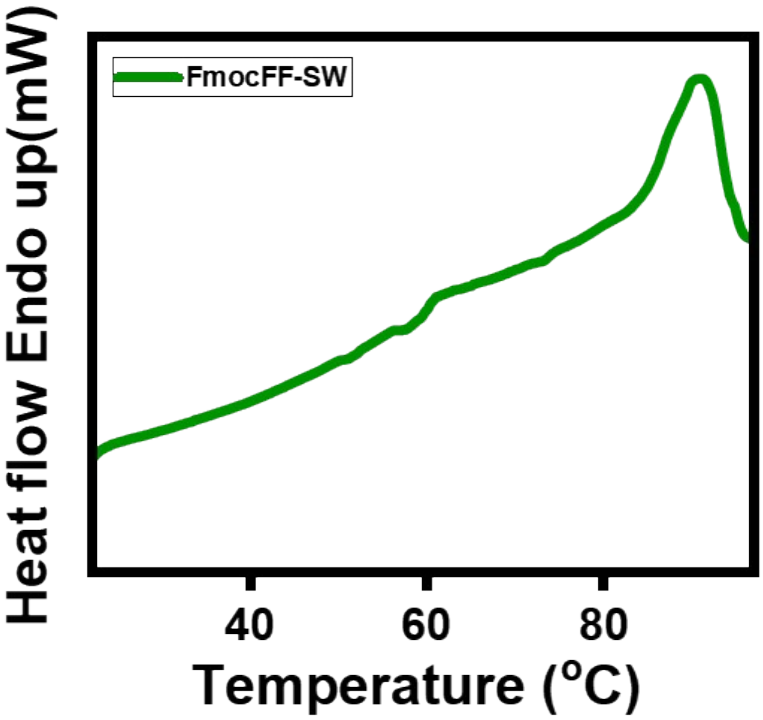

Fig. S21. Differential Scanning Calorimetry curve for FmocFF-SW hydrogel at 0.27% *w/v.*

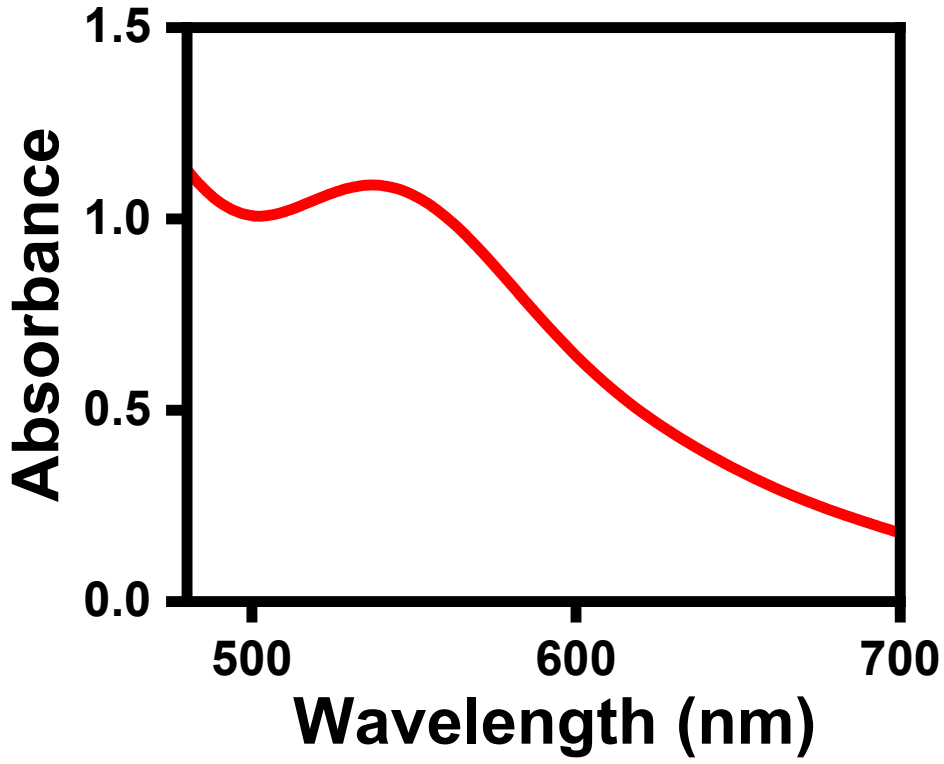

Fig. S22. Absorption spectra of Au NPs (final concentration of Au^{3+} solution 0.025% *w/v*), synthesized *in-situ* within the SS-SW hydrogel matrix prepared by heating the sample at 45°C.

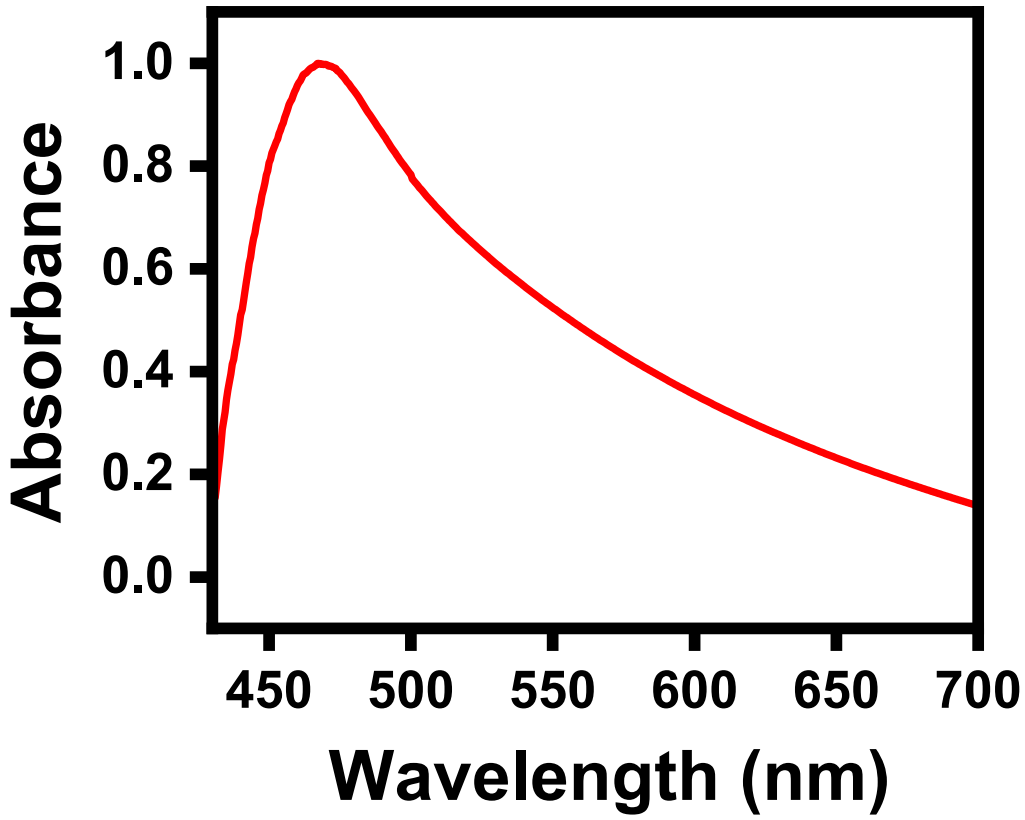

Fig. S23. Absorption spectra of Ag NPs (final concentration Ag^{+} solution 0.025% *w/v*), synthesized *in-situ* within SS-SW hydrogel matrix under diffused sunlight.

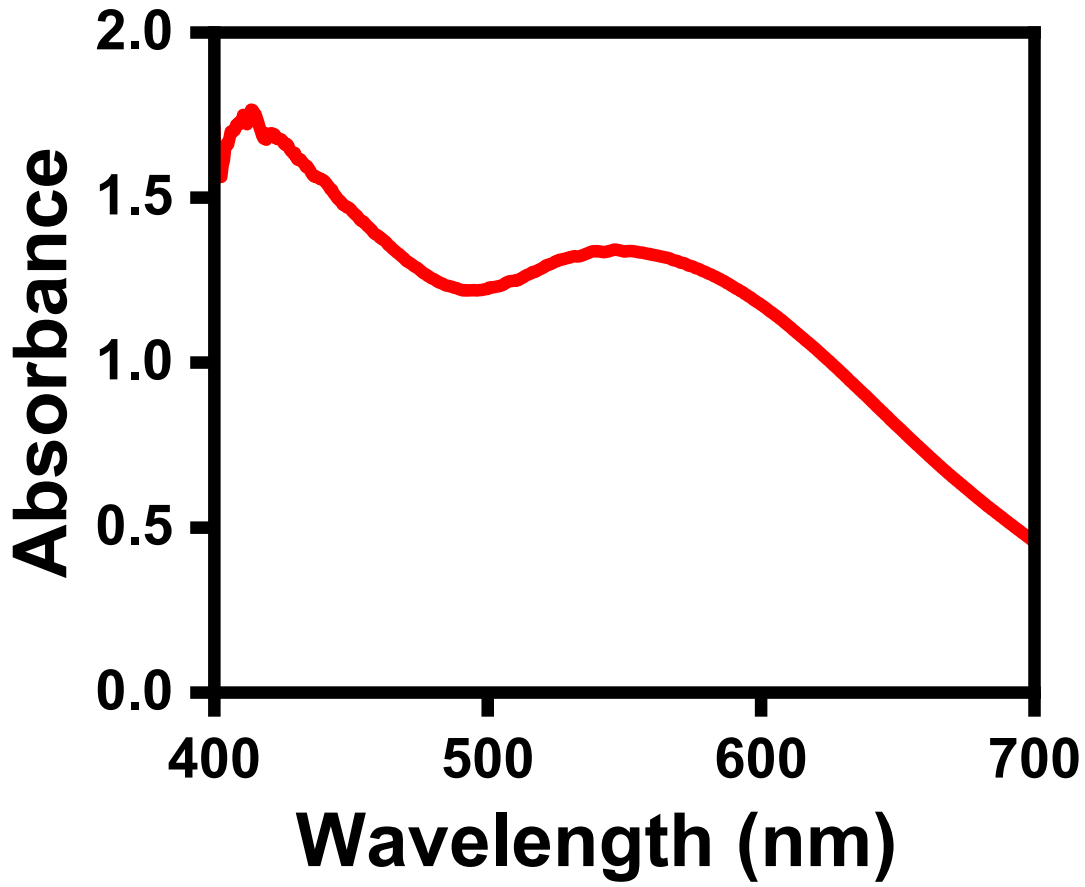

Fig. S24. Absorption spectra of Au/Ag NPs (final concentration of Au^{3+}/Ag^{+} solution = 0.025% *w/v*), synthesized *in-situ* within SS-SW hydrogel matrix under diffused sunlight, followed by heating at 45 °C.

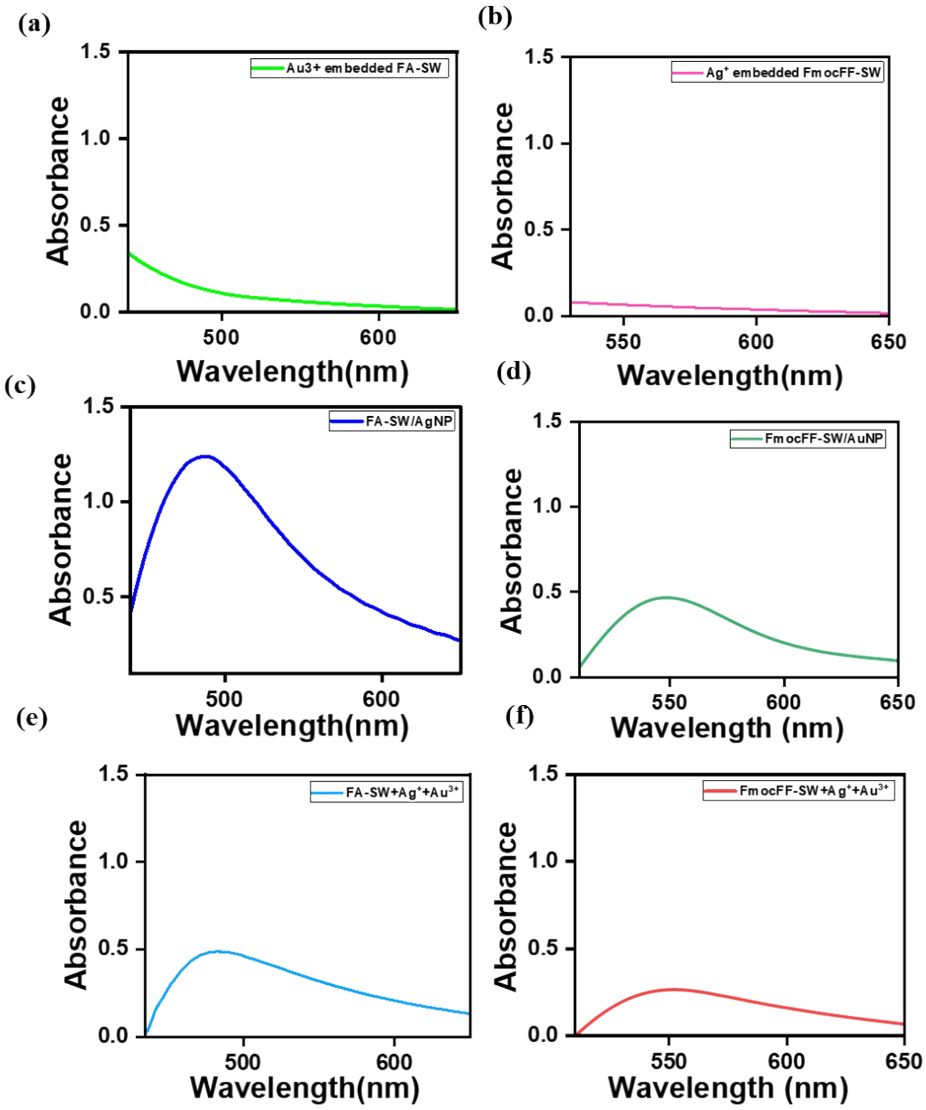

Fig. S25. Fig. S25. Absorption spectra of (a) Au^{3+} embedded FA-SW gel (b) Ag^{+} embedded FmocFF-SW gel (c) FA-SW/AgNPs (d) FmocFF-SW/AuNPs (e) FA-SW/AgNPs (Both Au^{3+} and Ag^{+} solution were employed, yet selective formation of Ag^{+} nanoparticle emerged within the gel) (f) FmocFF-SW/AuNPs (Both Au^{3+} and Ag^{+} solution were employed, yet selective formation of Au^{3+} nanoparticle emerged within the gel) (final concentration of metal solution = 0.025% w/v, synthesized in-situ within hydrogel matrix as discussed earlier in the experimental section, page 3).

Supporting Note 5: To clarify the origin of metal reduction and nanoparticle formation, we performed control experiments in which Ag, Au, and mixed Ag/Au systems were studied in individual FA and FmocFF gels using UV-vis spectroscopy (Figure S25).

Upon addition of individual metal ions, we observed that the FA-SW gel selectively facilitates the formation of Ag NPs, whereas the FmocFF-SW gel promotes the formation of Au NPs under identical experimental conditions. Notably, when a mixture of Ag^{+} and Au^{3+} ions was introduced into the individual gel systems, FA-SW gel continued to yield only Ag NPs, while FmocFF-SW gel exclusively produced Au NPs, with no evidence of bimetallic nanoparticle formation in either case.

These results clearly demonstrate that each gelator independently supports selective metal reduction, and importantly, that bimetallic Ag/Au NP formation is not achievable in the single-component systems. This strongly supports our conclusion that the self-sorted multicomponent network is essential for enabling the co-reduction and formation of bimetallic nanoparticles, likely by providing distinct yet spatially proximate reduction environments.

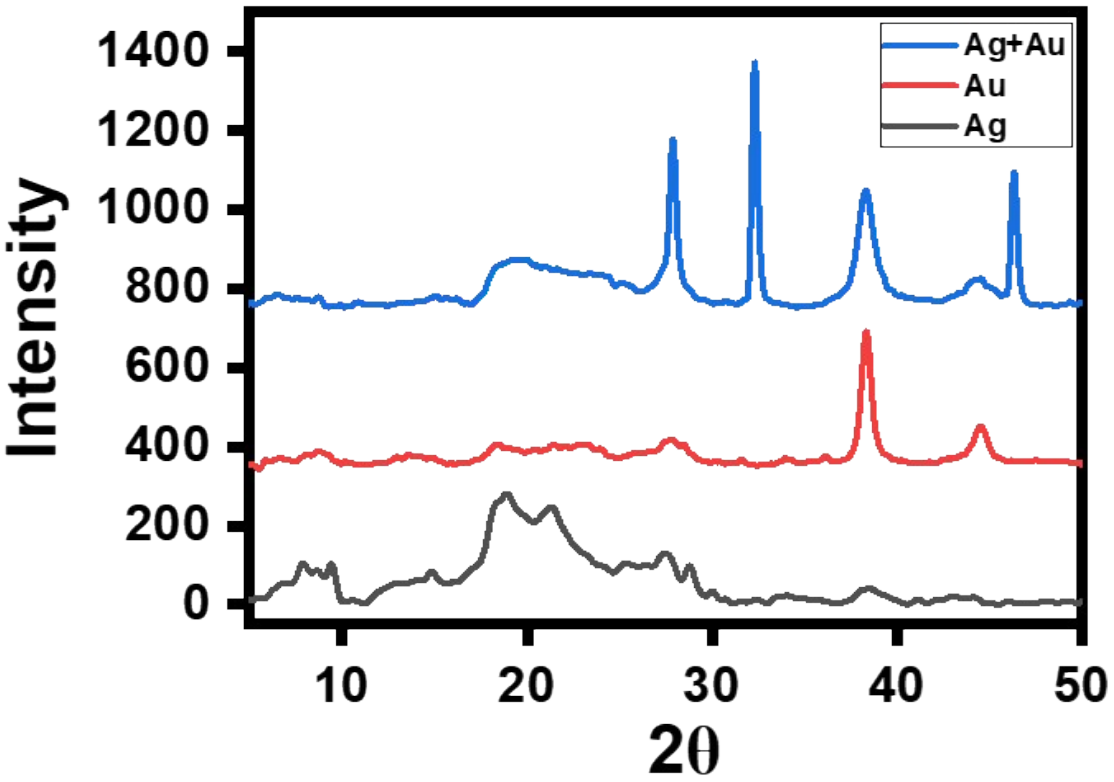

Fig. S26. Powder XRD spectra of the dried SS-SW gel sample prepared using Ag, Au, and Ag/Au NPs (concentration of both Au^{3+} and Ag^{+} solution 0.0125% *w/v*, total concentration = 0.025% *w/v*).

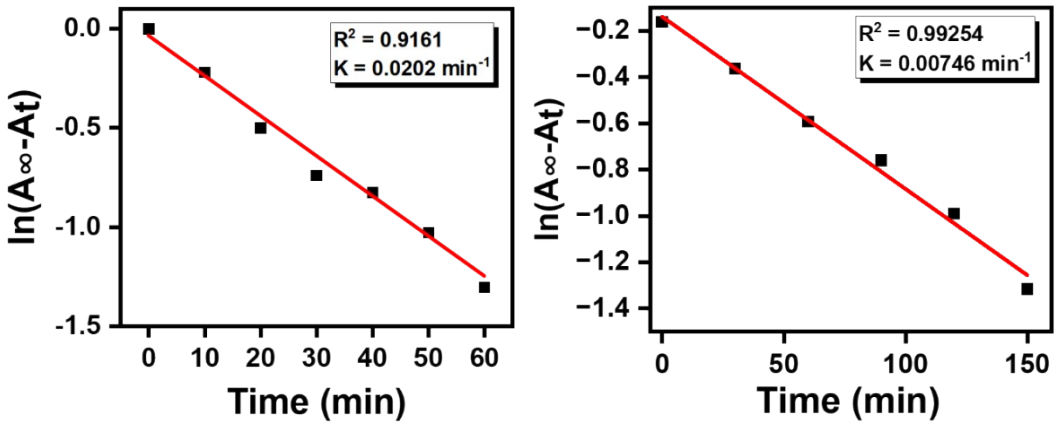

Fig. 27. Plot of ln(A∞ - At) versus t for (a) FA-SW/Ag hydrogel (0.23% w/v), and (b) FmocFF-SW/Au (0.05% w/v) hydrogel.

Supporting Note 6: Given the absence of external reducing agents, in both FmocFF and FA gels, the reduction of the metals is accomplished by the electron-rich functional groups and aromatic π-systems. Specifically, in FmocFF, the peptide backbone (-CONH-) and terminal -COOH groups, along with the π-electron-rich Fmoc aromatic moiety, can participate in electron-transfer processes. In FA-SW, the reduction process is primarily facilitated by multiple electron-donating sites, including -NH_2 and -COOH groups, as well as its pteridine ring, which is an electron-rich heteroaromatic system.[4-6] We note that the exact oxidation products are difficult to isolate and are likely to consist of partially oxidized or quinonoid-type species.

The reduction rate was calculated using UV-vis spectroscopy. For the FA-SW/Ag system, a 0.23% (w/v) gel of FA was prepared, and during preparation, 30 µL from stock silver nitrate solution (50 mM) was added. This gel was subjected to UV-vis measurement for the initial reading, after which it was placed under diffused sunlight. Subsequently, at 10 min intervals, UV-vis absorbance data (~490 nm) were collected until saturation was reached.

For the FmocFF-SW/Au system, a 0.05% (w/v) gel of FmocFF was prepared, and 30 µL $HAuCl_4$ solution (25 mM) was incorporated during the preparation. The absorption data (~548 nm) were recorded at 30 min intervals until saturation was reached.

The rate constant was then measured by the following equation [5]

$$\ln(A_\infty - A_t) = -kt + (A_\infty - A_0)$$

Where A_∞ is the absorbance at infinite time A_t is the absorbance at time t min and A_0 is the absorbance at time 0 min. From $\ln(A_\infty - A_t)$ vs t graph, we have calculated the rate constant, which is 0.0202 min^{-1} for FA-SW/Ag and 0.00746 min^{-1} for FmocFF-SW/Au.

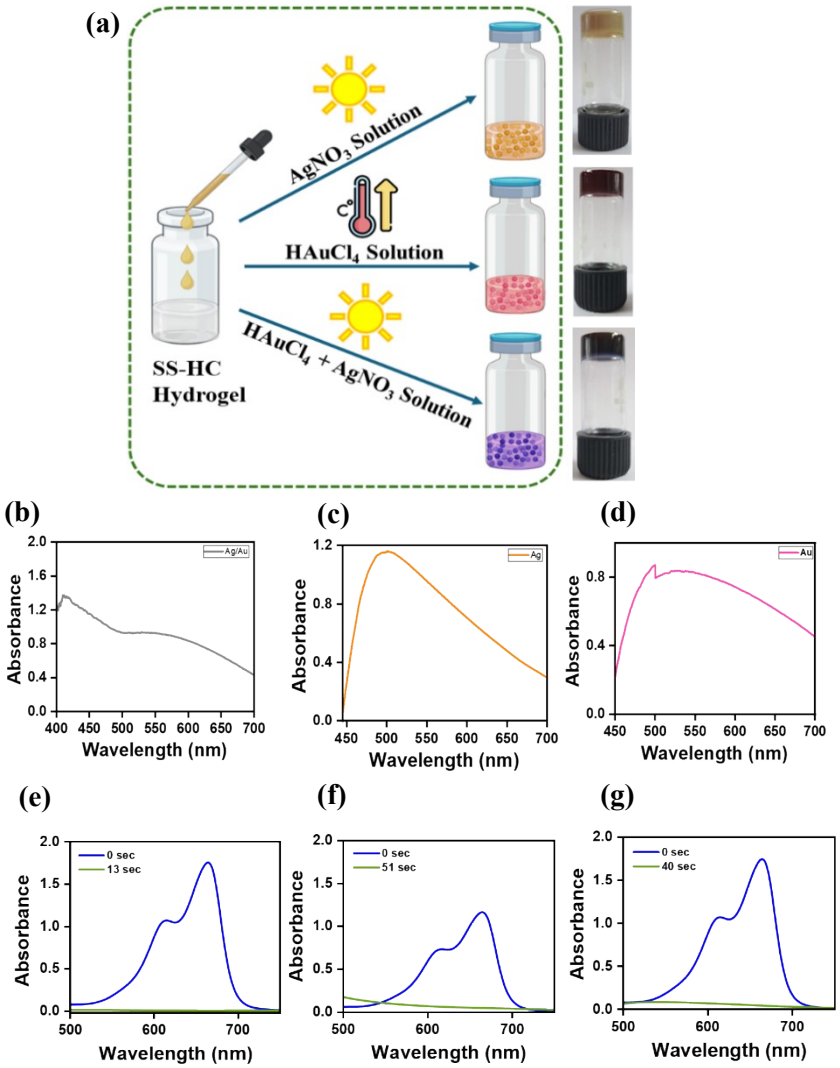

Fig. S28. (a) Schematic representation with digital images of the synthesis of in-situ Ag NPs, Au NPs, and Ag/Au NPs from SS-HC hydrogel. (b-d) Absorption spectra of (b) Ag/ Au NPs, (c) Ag NPs, and (d) Au NPs (final concentration of NP is 0.025% *w/v*), synthesized in-situ within the SS-HC hydrogel matrix (e-g) Absorption spectra for MB degradation in the presence of (e) Ag/ Au NPs, (f) Ag NPs and (g) Au NPs (final concentration of NP is 0.025% *w/v* and gel concentration 0.5% *w/v*) embedded in the SS-HC gel. The characteristic peak of MB observed at 664 nm vanishes upon its degradation in the presence of nano-hybrid gels (Au/Ag NPs = 13 sec, Au NPs = 40 sec, and Ag NPs = 51 sec). % Degradation of MB in the presence of (e) Au/Ag NPs = 99.89 %, (f) Ag NPs = 94.8 %, and (g) Au NPs = 97.4%.

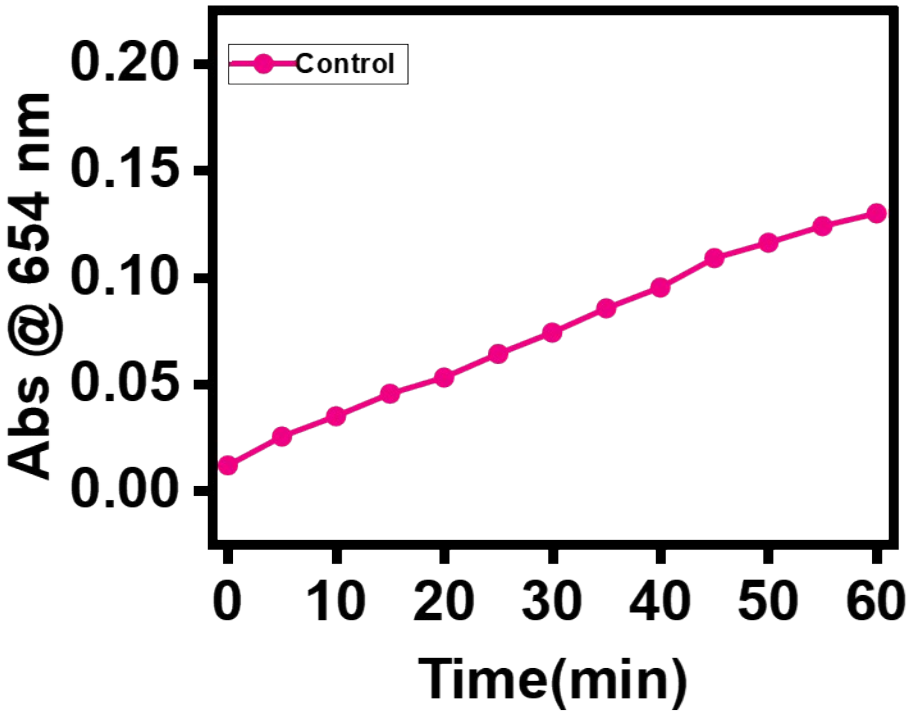

Fig. S29. UV-vis absorbance of control (without gel) during peroxidase activity measured at 654 nm. [Concentration of TMB = 0.5 mM, H_2O_2 = 5 mM] for 1 hr.

Table S3. Literature comparison of reported nano-metallic catalysts for peroxidase-activity with TMB substrate against their K_m and V_{max} values.

Catalyst	Substrate	K_m (mM)	V_{max} (10^{-8} Ms^{-1})	Reference
SS-SW/Ag/Au	**TMB**	**0.482**	**56.1**	**In this paper**
CNPs	**TMB**	**0.198**	**4.478**	**(7)**
GO-COOH	**TMB**	**0.0237**	**3.45**	**(8)**
HRP	**TMB**	**0.275**	**1.24**	**(8)**
Fe_3O_4 MNPs	**TMB**	**0.098**	**3.44**	**(1)**
Fe-Co alloy NPs	**TMB**	**1.79**	**4.56**	**(9)**
CeO_2 NPs	**TMB**	**3.8**	**70**	**(10)**
Pt nanoclusters	**TMB**	**0.63**	**270**	**(11)**
Au @ AgAu nanorattles	**TMB**	**1.65**	**200**	**(12)**

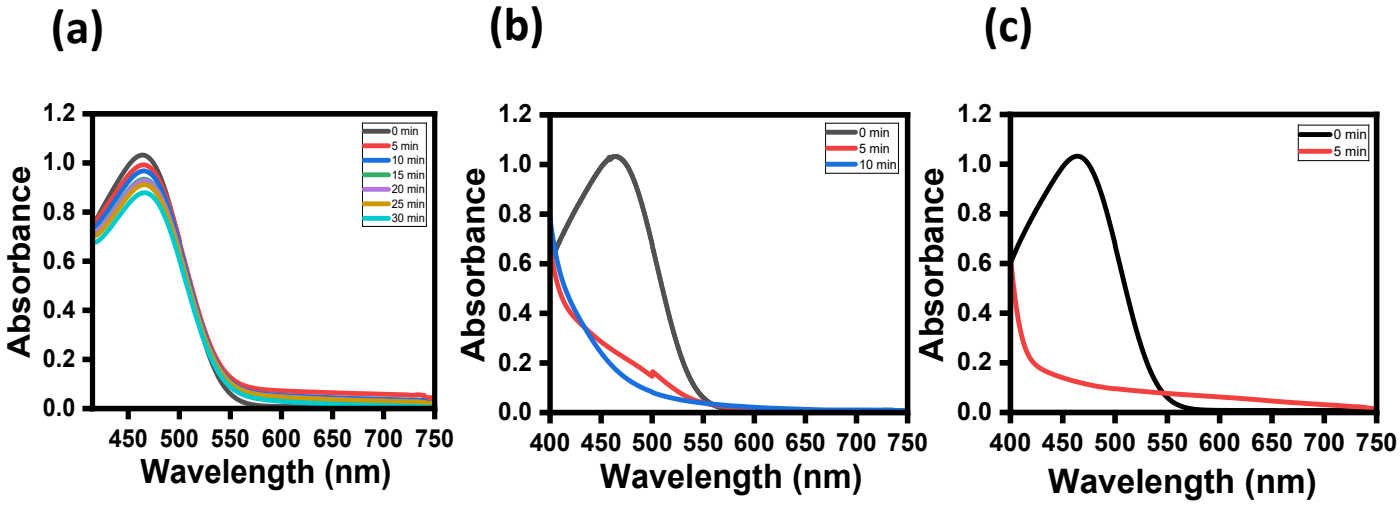

Fig. S30. Absorption spectra for methyl orange degradation in presence of (a) Ag NPs, (b) Au NPs and (c) Ag/Au NPs (final concentration of nanoparticle is 0.025% *w/v* and gel concentration 0.5% *w/v*), embedded in the SS-SW gel. The characteristic peak of methyl orange observed at 464 nm vanishes upon its degradation in presence of nano hybrid gels (Au/Ag NPs = 5 min, Au NPs = 10 min) for 30 mins. % Degradation of methyl orange in presence of (a) Ag NPs = 14.90%, (b) Au NPs = 82.65%, and (c) Au/Ag NPs = 88.07%.

Supporting Note 7. The degradation percentage was determined using the following equation: where C_0 and C represent the dye concentrations in the supernatant solution at initial time (0 min) and at time t, respectively, while A_0 and A denote the absorbance of the dye in the supernatant solution at times corresponding to 0 and t at λ_{max}

$$Degradation\ \% = \frac{C_0 - C}{C_0} \times 100\ \% = \frac{A_0 - A}{A_0} \times 100\ \%$$

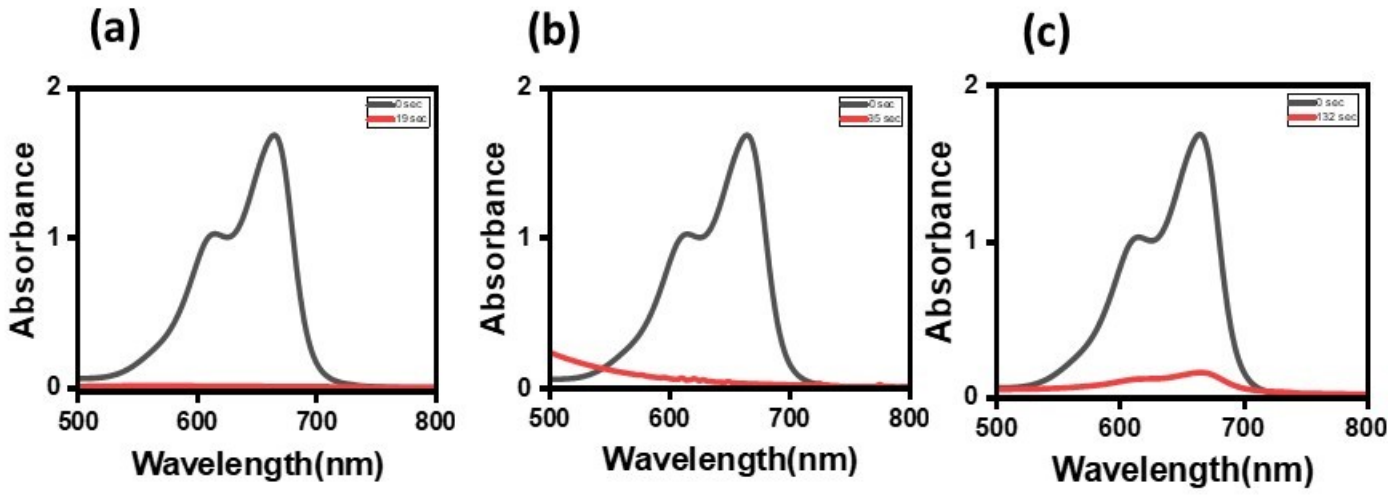

Fig. S31. Absorption spectra for methylene blue degradation in presence of (a) Ag NPs, (b) Au NPs and (c) Ag/Au NPs (final concentration 0.025% *w/v* and gel concentration 0.5% *w/v*) embedded in the SS-SW gel. The characteristic peak of methylene blue observed at 664 nm vanishes upon its degradation in presence of nano hybrid gels (Au/Ag NPs = 19 sec, Au NPs = 35 sec and Ag NPs = 132 sec) for 30 mins. % Degradation of methylene blue in presence of (a) Ag NPs = 90.38%, (b) Au NPs = 97.88%, and (c) Au/Ag NPs = 99.30%.

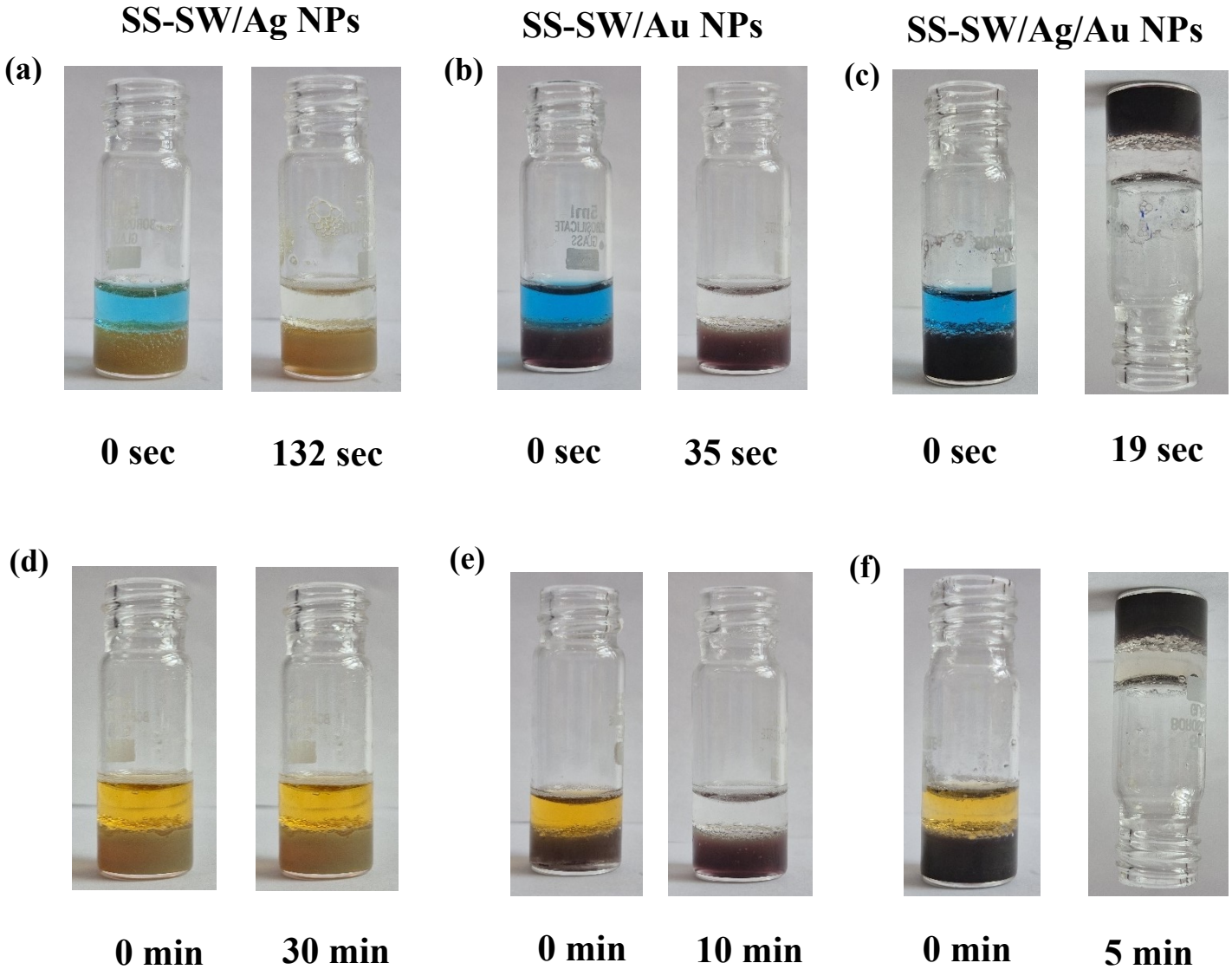

Fig. S32. (a-f) Digital images showing evidence of dye degradation before (at 0 min) and after addition of (a-c) MB solution with $NaBH_4$ in presence of (a) SS-SW/Ag NPs, (b) SS-SW/Au NPs, (c) SS-SW/Ag/Au NPs, and of (d-f) MO solution with $NaBH_4$ in presence of (d) SS-SW/Ag NPs, (e) SS-SW/Au NPs, (f) SS-SW/Ag/Au NPs.

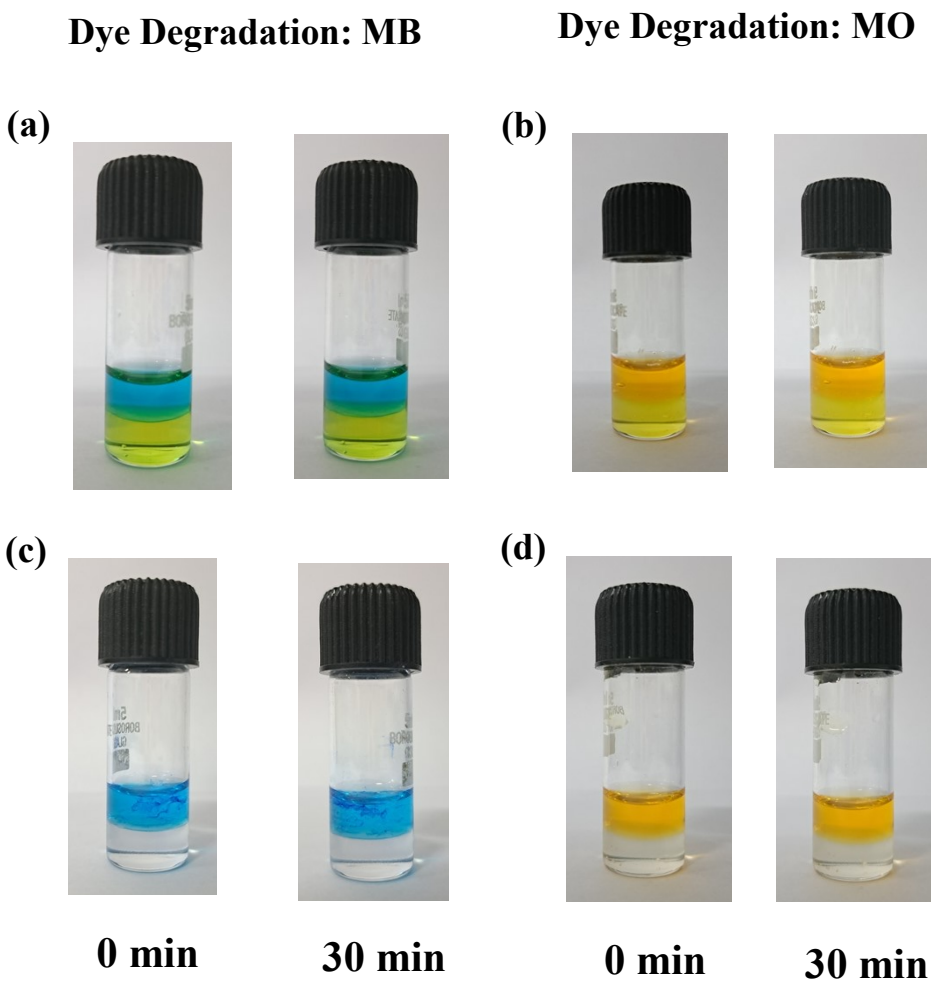

Fig. 33: Digital images showing dye degradation in FA-SW hydrogel (0.23% w/v, 1 mL) before (at 0 min) and after 30 mins of addition of (a) MB, and (b) MO solution in presence of $NaBH_4$. (c-d) Digital images showing dye degradation in FmocFF-SW hydrogel (0.27% w/v, 1mL) before (at 0 min) and after 30 mins of addition of (c) MB, and (d) MO solution in presence of $NaBH_4$.

Table S4. Comparison of average pH values before and after addition of $NaBH_4$ to pristine and multicomponent hydrogel samples in the presence and absence of NPs

Hydrogel	***Conc. of gel (% w/v)***	***pH before adding $NaBH_4$***	***pH after adding $NaBH_4$***
FmocFF-SW	0.27	3.8 ± 0.1	4.02 ± 0.6
FA-SW	0.23	4.13 ± 0.3	4.18 ± 0.54
SS-SW	0.5	3.96 ± 0.9	4.00 ± 0.8
SS-SW/Ag	0.5	2.94 ± 0.21	3.02 ± 0.2
SS-SW/Au	0.5	2.89 ± 0.3	2.75 ± 0.1
SS-SW/Ag/Au	0.5	2.62 ± 0.51	2.53 ± 0.8

Evidently, the addition of $NaBH_4$ does not significantly alter the pH of the gels. Additionally, we did not observe any gel degradation during the reaction, indicating the gel's stability in the presence of $NaBH_4$.

References

1. L. Gao, J. Zhuang, L. Nie, J. Zhang, Y. Zhang, N. Gu, T. Wang, J. Feng, D. Yang, S. Perrett and X. Yan, *Nat. Nanotechnol*., 2007, **2**, 577–583.
2. P. Makam, S. S. R. K. C. Yamijala, K. Tao, L. J. W. Shimon, D. S. Eisenberg, M. R. Sawaya, B. M. Wong and E. Gazit, *Nat. Catal*., 2019, **2**, 977–985.
3. S. Buzrul, *Chem. Biodivers*. 2026, **23**, e03211.
4. V. V. Adole, G. Mishra and P. Chakraborty, *ACS Appl. Nano Mater*., 2025, **8**, 19535–19548.
5. I. Sahu, J. Verma, A. K. Bera, S. Pande, A. Bhavsar, F. Pati and P. Chakraborty, *ACS Appl. Mater. Interfaces*, 2024, **16**, 34141–34155.
6. K. A. Rawat, R. K. Singhal, and S. K. Kailasa, Sens. Actuators B: Chem. 2017, 249, 30-38.
7. L. Chen, X. Li, Z. Li, K. Liu and J. Xie, *RSC Adv*., 2022, **12**, 595–601.
8. Y. Song, K. Qu, C. Zhao, J. Ren and X. Qu, *Adv. Mater.*, 2010, **22**, 2206–2210.
9. Y. Chen, H. Cao, W. Shi, H. Liu and Y. Huang, *Chem. Comm*., 2013, **49**, 5013.
10. Asati, S. Santra, C. Kaittanis, S. Nath and J. M. Perez, *Angew. Chem.*, 2009, **121**, 2344–2348.
11. C.-J. Yu, T.-H. Chen, J.-Y. Jiang and W.-L. Tseng, *Nanoscale,* 2014, **6**, 9618–9624.
12. F. G. da Silva, E. V. Formo and P. H. C. Camargo, *Dalton Trans*., 2022, **51**, 15133–15141